iScience

Article

# APE1 promotes lung adenocarcinoma through G4-mediated transcriptional reprogramming of urea cycle metabolism

## Graphical abstract

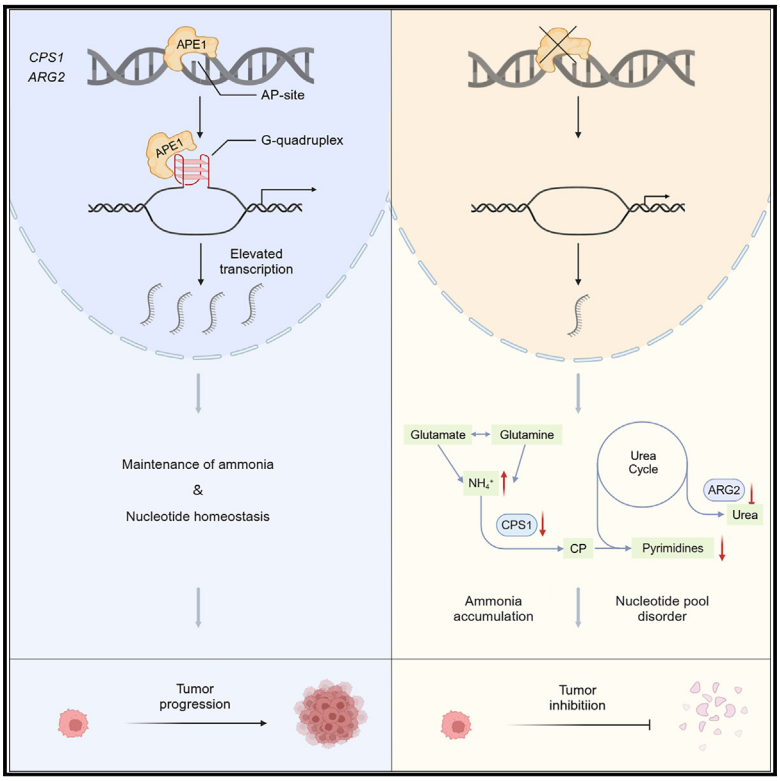


## Highlights

- APE1 is required to sustain *Kras*$^{G12D}$ -induced LUAD development
- APE1 reprograms the urea cycle and pyrimidine metabolism in LUAD
- APE1 promotes *CPS1* and *ARG2* transcription by modulating the presence of G4 structures
- CPS1 restoration mitigates DNA damage and proliferation defects in *APE1*$^{-/-}$ LUAD

## Authors

Yanhao Yu, Chaochao Cen, Zhenyu Shao, ..., Hongbin Ji, Guoliang Xu, Yarui Du

## Correspondence

yrdu@sibcb.ac.cn

## In brief

Biological sciences; Molecular biology; Cell biology

Yu et al., 2025, iScience *28*, 112275
May 16, 2025 
https://doi.org/10.1016/j.isci.2025.112275

CellPress

iScience

CellPress
OPEN ACCESS

Article

# APE1 promotes lung adenocarcinoma through G4-mediated transcriptional reprogramming of urea cycle metabolism

Yanhao Yu,[1,4] Chaochao Cen,[1,4] Zhenyu Shao,[1] Chaohan Wang,[1] Yiqin Wang,[1] Zongjie Miao,[1] Meiling Sun,[1] Chao Wang,[1] Qing Xu,[1] Kaiwei Liang,[2] Jiaxin Zhou,[1] Dan Zhou,[3] Hongbin Ji,[1] Guoliang Xu,[1,3] and Yarui Du[1,5,*]

[1]CAS Key Laboratory of Epigenetic Regulation and Intervention, Shanghai Key Laboratory of Molecular Andrology, Shanghai Institute of Biochemistry and Cell Biology, Center for Excellence in Molecular Cell Science, University of Chinese Academy of Sciences, Chinese Academy of Sciences, Shanghai 200031, China

[2]School of Basic Medical Sciences, Wuhan University, Wuhan 430072, China

[3]Shanghai Key Laboratory of Medical Epigenetics, Institutes of Biomedical Sciences, Chinese Academy of Medical Sciences (RU069) & Zhongshan-Xuhui Hospital, Medical College of Fudan University, Shanghai 200032, China

[4]These authors contributed equally

[5]Lead contact

*Correspondence: yrdu@sibcb.ac.cn

https://doi.org/10.1016/j.isci.2025.112275

## SUMMARY

Lung adenocarcinoma (LUAD) remains the leading cause of cancer deaths worldwide. Apurinic/apyrimidinic endonuclease 1 (APE1), an enzyme integral to DNA repair and redox signaling, is notably upregulated in LUAD. Here we reveal that APE1 amplification, primarily via allele duplication, strongly correlates with poor prognosis in LUAD patients. Using human LUAD cell lines and a *KRAS*-driven mouse model, we showed that *APE1* deletion hampered cell proliferation and tumor growth, highlighting its role in tumorigenesis. Mechanistically, APE1 promoted the transcription of urea cycle genes *CPS1* and *ARG2* by modulating the presence of G-quadruplex (G4) structures in their promoter regions. APE1 loss disrupted the urea cycle and pyrimidine metabolism, inducing metabolic reprogramming and growth arrest, which could be rescued by CPS1 or pyrimidine restoration. These findings uncover APE1's role in transcriptional regulation of urea cycle metabolic reprogramming via G4 structure, providing a potential therapeutic target LUAD patients with elevated APE1 expression.

## INTRODUCTION

Lung cancer remains as the leading cause of cancer-related mortality worldwide, accounting for 21% of all cancer deaths in 2023, and exhibits high incidence and high mortality with a 10%–15% 5-year survival rate.[1] Non-small-cell lung cancer (NSCLC) comprises approximately 85% of all lung cancer cases, with lung adenocarcinoma (LUAD) emerging as the predominant histologic subtype.[2] Multiple oncogenic driver mutations have been identified in LUAD, including *KRAS*, *EGFR*, and *BRAF* mutations. Notably, *KRAS* mutations are prevalent, accounting for a large proportion (32%) of LUAD cases, with a majority of mutations occurring at codon 12 (85%).[3,4] Considering the allele specificity and pivotal roles of KRAS mutants in various cellular processes, novel strategies in a KRAS allele-dependent manner are still required.

Over the past two decades, although chemotherapy and targeted treatments have significantly improved patient prognosis, the emergence of acquired drug resistance remains a significant barrier to cancer treatment.[5] An elevated DNA repair capacity in cancer cells is thought to contribute to the development of resistance against radiation and platinum-based chemotherapy.[6,7] Notably, human apurinic/apyrimidinic endonuclease 1 (APE1) has been observed with elevated expression level in various cancers, including bladder cancer,[8] non-small cell lung carcinoma,[9,10] glioma,[11] pancreatic cancer,[12] cervical cancer,[13,14] prostate cancer,[14] and ovarian cancer.[15] The blockade of APE1 activity by inhibitors has been proven to induce lethality in breast cancer susceptibility (BRCA) and ataxia telangiectasia mutated (ATM) deficient cells.[16] Moreover, elevated APE1 level are associated with increased resistance to chemotherapy and radiotherapy, leading to poor clinical outcomes,[17,18] and silencing APE1 expression can sensitize cancer cells to chemotherapy and radiation treatment.[19,20] Consequently, APE1 is considered a promising prognostic cancer biomarker and a potential therapeutic target.

APE1 was originally identified as an apurinic/apyrimidinic (AP) endonuclease.[21] In mammalian cells, APE1 dominates the cleavage of over 95% of AP site lesions, playing a vital role in protecting cells from DNA damage caused by internal or external factors.[22] The conserved Asn212 residue (Asn211 in mice) is indispensable for the enzymatic activity of APE1.[23,24] Besides

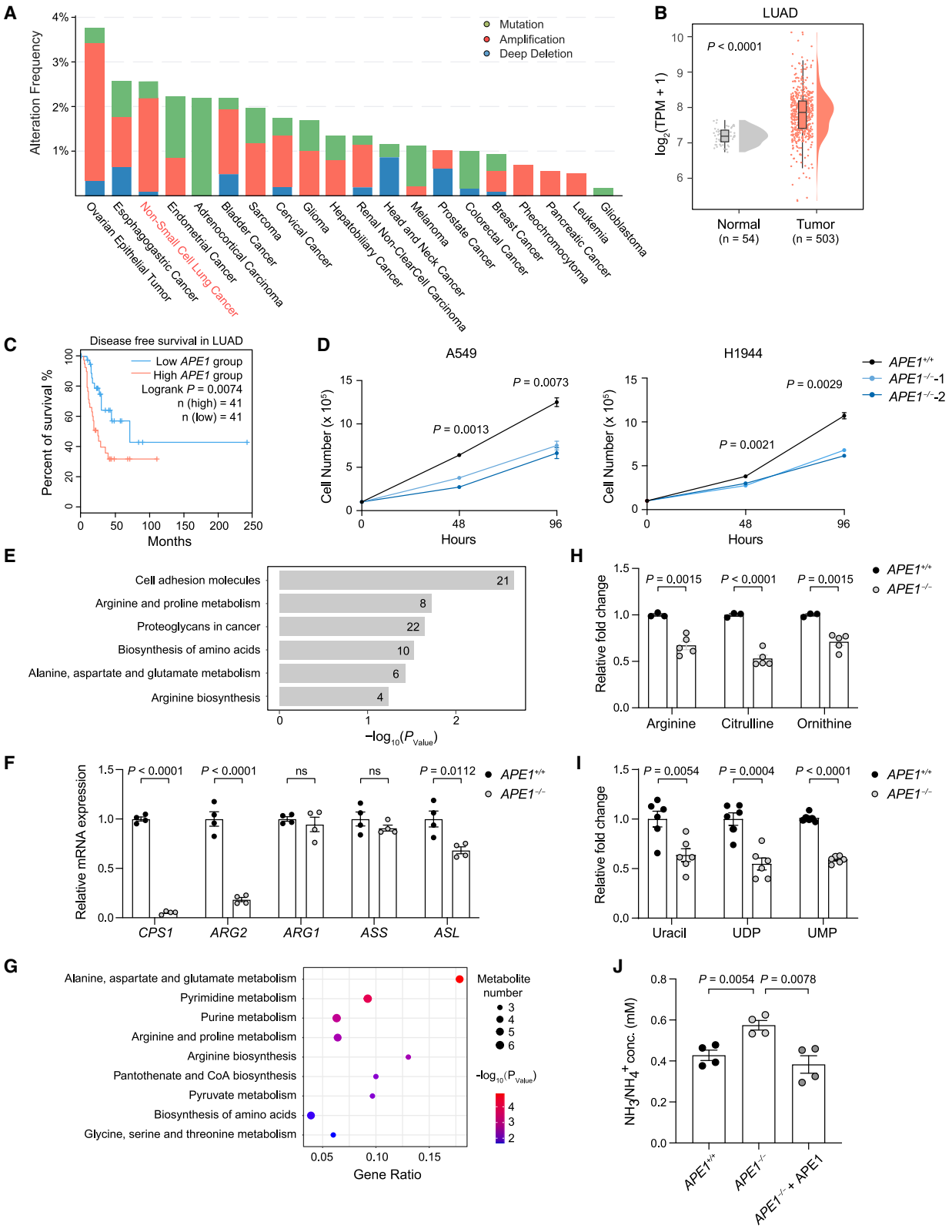


(legend on next page)

its role in DNA repair, APE1 also functions as a redox signaling hub regulating critical transcription factors (TFs), including Egr1, nuclear factor κB (NF-κB), p53, and HIF1a.[25,26] Through thiol/sulfide exchange on cysteine residue, APE1 reduces oxidized TFs to their active forms, enabling these activated TFs to bind to DNA.[27] This redox activity endows APE1 with the capacity to modulate gene expression and participate in many cellular processes, including growth, inflammation, and angiogenesis.[28,29] The redox activity of APE1 primarily relies on Cys65, a cysteine residue located in its N-terminal tail, and operates independently of APE1's DNA repair function.[30] Recent studies have revealed an additional role of APE1 in controlling the formation of higher-order DNA secondary G-quadruplex (G4) structures to regulate transcription.[31] Specifically, APE1 plays critical roles in stabilizing G4 structures and promoting *KRAS* expression in pancreatic ductal adenocarcinoma (PDAC).[32] These discoveries have suggested the diverse functions of APE1, expanding its role beyond just DNA repair to include transcriptional regulation and modulation of G4 structures.

Although emerging evidence has established a correlation between elevated APE1 expression and unfavorable outcomes, such as poor prognosis, invasion, and chemo-resistance,[33] the specific function and precise mechanism of APE1 in the progression of LUAD tumors remain elusive. In this study, we elucidate the role of APE1 in the malignant progression of LUAD through the transcriptional regulation of urea cycle genes, offering potential therapeutic strategies for LUAD patients.

## RESULTS

### Elevated APE1 expression correlates with malignancy in human LUAD

Analyses of cBioPortal database showed that about 2.5% NSCLS patients harbored genomic alterations in *APE1*, with 80% of these alterations being allele amplification (Figure 1A). Correspondingly, the transcriptional level of *APE1* was significantly higher in LUAD tumor tissues compared to normal tissues (Figure 1B). Notably, high *APE1* expression was evidently linked with poor patient survival (Figure 1C). LUAD exhibits *KRAS* mutation in approximately 32% of cases.[34] We then employed CRISPR-Cas9-mediated *APE1* knockout in two *KRAS*-mutant human LUAD cell lines, A549 and H1944 cells, to examine the effect of APE1 loss ($APE1^{-/-}$). The deletion of APE1 was confirmed at both DNA and protein levels (Figures S1A–S1D). We found that APE1 deletion significantly inhibited cell proliferation of A549 and H1944 cells (Figure 1D). These findings indicate that APE1 might play an oncogenic role in LUAD.

### APE1 transcriptionally reprogramed the urea cycle and pyrimidine metabolism in LUAD

As APE1 has been demonstrated to regulate *KRAS* transcription in PDAC,[32] we investigated the involvement of APE1 in the regulation of *KRAS* expression in LUAD. In contrast to its role in PDAC, APE1 deletion did not affect KRAS expression at either mRNA or protein levels in A549 cells (Figures S1E and S1F), consistent with previously published RNA sequencing (RNA-seq) data (Figure S1G). This observation suggests that APE1 regulation may be specific to the type of cancer. To uncover the mechanism underlying the anti-tumor effect of APE1 deletion, we performed RNA-seq analysis on APE1-deleted cells. Principal-component analysis (PCA) revealed the clear clustering of A549 and H1944 cells based on their genotypes (Figures S2A and S2C). Remarkably, Kyoto Encyclopedia of Genes and Genomes (KEGG) analysis of the differentially expressed genes (DEGs) showed significant enrichments in terms related to the biosynthesis of amino acids, particularly arginine biosynthesis in A549 and H1944 cell lines (Figures 1E and S2D). Gene set enrichment analysis (GSEA) further confirmed the dysregulation of biosynthesis and activation of amino acid pathways (Figure S2B). Many cancer cells exhibit dysregulated expression of urea cycle enzymes,[35] including carbamoyl phosphate synthetase 1 (CPS1), argininosuccinate synthase (ASS1), argininosuccinate lyase (ASL), arginase 1 (ARG1), and arginase 2 (ARG2) (Figure S2E). Of note, the expression of *CPS1* and *ARG2* was downregulated in both A549 and H1944 cells with APE1 deletion, as evidenced by RT-qPCR results (Figures 1F and S2F). Next, we performed untargeted metabolomics analysis to assess the metabolic alterations in $APE1^{-/-}$ A549 cells by UHPLC-MS/MS. KEGG analysis indeed revealed the enrichment of altered metabolites in amino acid and nucleoside metabolism pathways (Figures 1G, S2G and S2H). Notably, the urea cycle metabolites, including citrulline, arginine, and ornithine, were

**Figure 1. APE1 amplification drives urea cycle reprogramming and promotes tumor progression in LUAD**

(A) Global view of the somatic genome alterations in APE1 in pan-cancer. This figure is adapted from an OncoPrint figure generated by cBioPortal.

(B) Boxplots showing *APE1* mRNA expression levels in LUAD compared with normal adjacent tissues. Clinical expression data of *APE1* mRNA were derived from GEPIA.

(C) Kaplan-Meier curves showing overall survival of LUAD patients stratified by *APE1* mRNA levels. Source data can be found from GEPIA.

(D) Cell growth curve of human cancer cell lines A549 and H1944 with *APE1* deletion ($APE1^{-/-}$) or not ($APE1^{+/+}$). Two independent knockout clones in each cell line are presented.

(E) KEGG pathway analysis of the differentially expressed genes (DEGs) in A549 cells upon APE1 knockout. DEGs are defined by 1.5-fold change and adjusted *p* value $\leq$0.05. The number of genes in each category is indicated.

(F) RT-qPCR analysis of urea cycle genes in $APE1^{+/+}$ and $APE1^{-/-}$ A549 cells. Data are presented as mean ± SEM from four biological replicates.

(G) KEGG pathway analysis of metabolites with aberrant levels in $APE1^{-/-}$ A549 cells. KEGG enrichment pathways are defined by adjusted *p* value $\leq$0.05.

(H and I) Relative abundance of urea cycle intermediates arginine, ornithine, and citrulline (H) and pyrimidines (I) in $APE1^{+/+}$ and $APE1^{-/-}$ A549 cells measured by UHPLC-MS/MS. UDP, uridine 5′-diphosphate; UMP, uridine 5′-monophosphate. Data are presented as mean ± SEM from five or six biological replicates.

(J) Ammonia/ammonium levels of $APE1^{+/+}$ and $APE1^{-/-}$ A549 cells with or without restoration of APE1. Data are presented as mean ± SEM from four biological replicates. The expression levels were normalized to *GAPDH*, and then compared to the $APE1^{+/+}$ control, which was set to 1.0.

Statistical significance was assessed using two-sided log rank test (C), two-way ANOVA (D), and two-tailed unpaired Student's t test (F, H–J). ns, not significant.

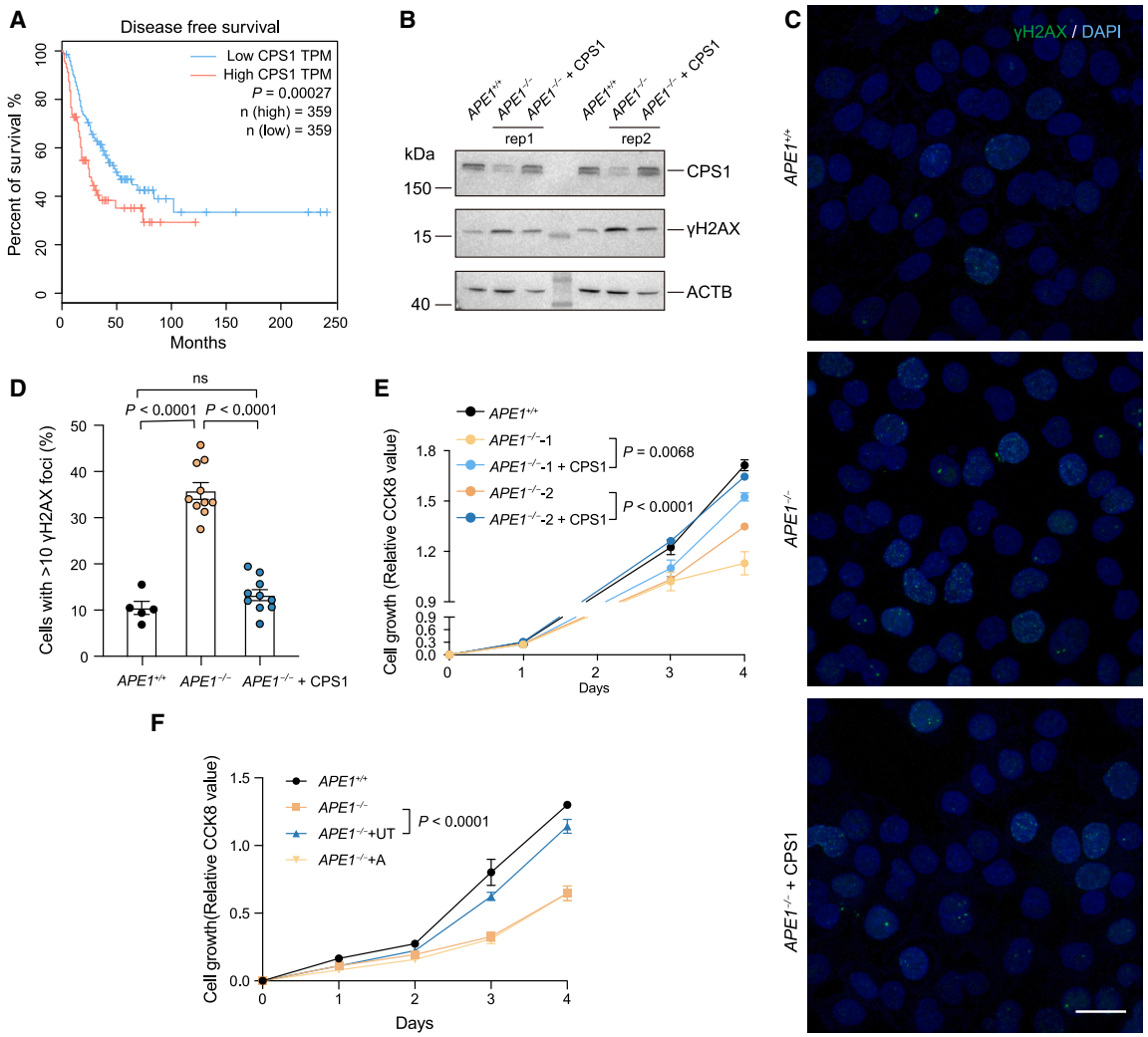


**Figure 2. CPS1 restoration alleviates DNA damage and proliferation defects of *APE1*$^{-/-}$ LUAD**

(A) Kaplan-Meier curves showing overall survival of *CPS1*-high (the highest 25%) or *CPS1*-low (the remaining 75%) LUAD patients classified based on *CPS1* mRNA levels. The source data is accessible through GEPIA.

(B) Western blot analysis of CPS1 and γH2AX in wildtype (*APE1*$^{+/+}$), APE1 knockout (*APE1*$^{-/-}$) and APE1 knockout with the restoration of CPS1 (*APE1*$^{-/-}$ + CPS1) A549 cells. ACTB was detected as a loading control.

(C) Representative immunofluorescence images of A549 cells with the indicated genotypes stained with anti-γH2AX (green) and DAPI (blue) from two independent experiments. Scale bar indicates 20 μm.

(D) Percentage of cells with greater than 10 γH2AX foci in *APE1*$^{+/+}$ and *APE1*$^{-/-}$ A549 cells with or without restoration of CPS1. Five representative images for *APE*$^{+/+}$ and ten representative images for *APE1*$^{-/-}$ or *APE1*$^{-/-}$ + CPS1 group form two independent experiments were counted, respectively.

(E) Cell growth curves of *APE1*$^{-/-}$ A549 cells with or without restoration of CPS1.

(F) Effect of supplementing uridine and thymidine (UT) or adenosine (A) on cell proliferation rate in *APE1*$^{-/-}$ A549 cells.

Data in (E) and (F) presented as mean ± SEM from three biological replicates. The data in (B) and (E) are derived from two independent CRISPR clones. Statistical significance was assessed using two-sided log rank test (A), two-tailed unpaired Student's t test (D), or two-way ANOVA (E and F). ns, not significant.

decreased (Figure 1H). Moreover, the level of pyrimidine decreased along with an increase in purine levels (Figures 1I and S2I). To determine how urea cycle metabolism affects tumor growth, we measured ammonia level in A549 cells with or without APE1. Our data showed that APE1 deletion promoted ammonia accumulation, which could be reversed by APE1 overexpression (Figure 1J). Taken together, these data suggest that APE1 deletion affects lung cancer cell proliferation potentially through reprogramming the urea cycle metabolism.

## CPS1 restoration alleviates DNA damage and proliferation defects of *APE1*$^{-/-}$ LUAD

Interestingly, we found that abundant *CPS1* mRNA correlated with poor prognosis in LUAD (Figure 2A), suggesting a potential pivotal role for CPS1 in the progression of LUAD malignancy. Indeed, CPS1 expression was reduced at the protein level in *APE1*$^{-/-}$ A549 cells (Figure 2B). CPS1, a rate-limiting enzyme within the urea cycle, is necessary to maintain pyrimidine pools and DNA synthesis in lung cancer cells.[36] Consistently, we

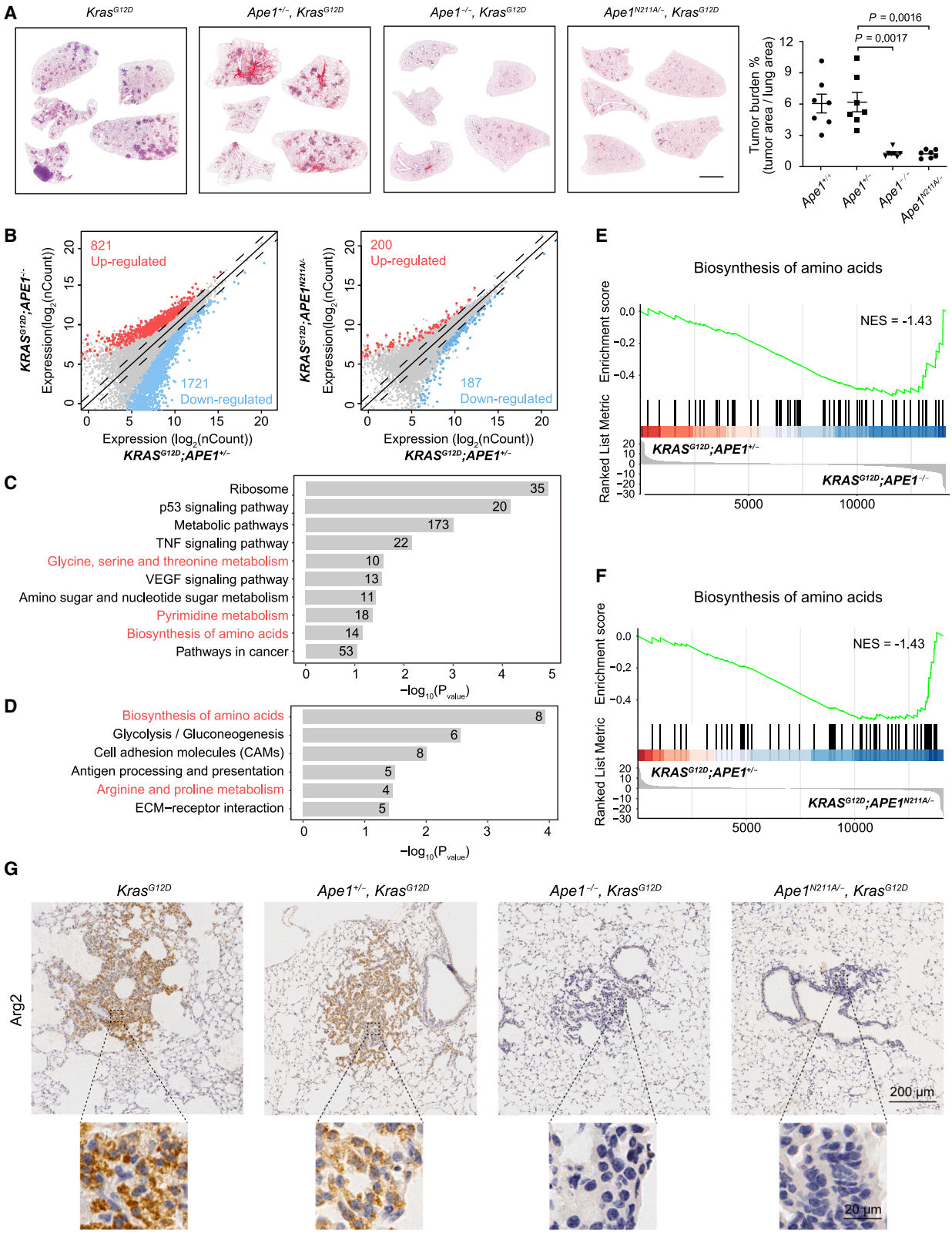


*(legend on next page)*

observed significant cell-cycle arrest in the G0/G1 phase (Figure S2J) and increased double-strand DNA breaks (DSBs) in *APE1*$^{-/-}$ cells (Figures 2C and 2D). To confirm the role of CPS1 in LUAD malignancy, we restored CPS1 expression or supplemented exogenous uridine (U) and thymidine (T) in *APE1*$^{-/-}$ A549 cells and observed a reduction in DNA damage and restoration of cell proliferation (Figures 2B–2F). These findings provide compelling evidence that the decreased expression of CPS1 contributes to DNA damage and proliferation defects in *APE1*$^{-/-}$ cells.

## APE1 is required to sustain *Kras*$^{G12D}$-induced LUAD development in mice

To verify the functional importance of APE1 in LUAD development *in vivo*, we utilized the *Kras*-driven autochthonous genetically engineered mouse model (GEMM) (Figure S3A) and generated the Ape1 conditional knockout and N211A mutant mice. To establish a conditional knockout mouse model for Ape1, we inserted two *loxP* sites flanking exon 2 and exon 3 of the *Ape1* gene (Figures S3B–S3D). Additionally, considering the importance of Asn211 for the AP endonuclease activity of mouse APE1 protein,[23,24] we generated the N211A mutant mice through CRISPR-Cas9-mediated homologous recombination (Figures S3E and S3F). We obtained the following four cohorts: *Kras*$^{LSL\text{-}G12D/+}$, *Kras*$^{LSL\text{-}G12D/+}$; *Ape1*$^{flox/+}$, *Kras*$^{LSL\text{-}G12D/+}$; *Ape1*$^{flox/flox}$, and *Kras*$^{LSL\text{-}G12D/+}$; *Ape1*$^{flox/N211A}$. In these models, the induction of Ape1 deletion and the expression of oncogenic *Kras*$^{G12D}$ in lung epithelial cells to initiate lung tumorigenesis were achieved through intranasal infection with a Cre-expressing adenovirus under the control of CMV promoter (Ad-CMV-Cre) (Figure S3G) as previously reported.[34]

Consistent with our findings in human cancer cell lines, Ape1 deletion in mice reduced tumor burden by 80% compared to wild-type (*Ape1*$^{+/+}$) and Ape1 heterozygotes (*Ape1*$^{+/-}$) at 17 weeks post Ad-Cre instillation (Figures 3A and 3B), further confirming the promotive role of APE1 in LUAD development. Notably, the inhibition of tumor progression in Ape1-knockout mice was dependent on the AP endonuclease activity of Ape1, as Ape1$^{N211A/-}$ mice phenocopied the Ape1 KO mice (Figures 3A and 3B). To further confirm the oncogenic role of APE1, and validate the role of its AP endonuclease activity in LUAD development *in vivo*, we generated lentiviruses expressing both Cre recombinase and either wild-type (WT) Ape1, which could mimic Ape1 allele amplification, or the N211A mutant for administration into *Kras*$^{LSL\text{-}G12D/+}$ mice (Figure S4A). We found that, the expression of WT APE1, but not the N211A mutant, strongly potentiated Kras$^{G12D}$-driven LUAD development (Figures S4B and S4C). Thus, these results demonstrate that the AP endonuclease activity of Ape1 is required to promote LUAD development.

Next, we sorted tdTomato$^{+}$/EPCAM$^{+}$/DAPI$^{-}$/CD45$^{-}$/CD31$^{-}$ lung epithelial cells 12 weeks after Ad-Cre instillation and performed RNA-seq to profile transcriptional changes. Although the number of DEGs in *Ape1*$^{N211A/-}$ versus *Ape1*$^{+/-}$ cells was smaller than that in *Ape1*$^{-/-}$ versus *Ape1*$^{+/-}$ cells (Figure 3B), both groups showed significant enrichment of pathways related to amino acid biosynthesis (Figures 3C–3F). Furthermore, we confirmed the decreased expression of Arg2 in Ape1 KO and N211A mutant lung tumor sections through immunohistochemistry (Figure 3G). Together, these findings pointed to the critical roles of urea cycle in sustaining tumor progression and a functional interplay between APE1 and urea cycle reprograming in LUAD development.

## APE1 is involved in G4-mediated transcription of *CPS1* and *ARG2*

Analysis of the human LUAD datasets from The Cancer Genome Atlas (TCGA) database revealed that both *CPS1* and *ARG2* positively correlated with *APE1* expression (Figure S5A), consistent with the trends observed in our experiments (Figures 1 and 3). Given that APE1 is involved in G4-mediated gene expression,[31] we then investigated whether the promoter regions (TSS +/− 1 kb) of *CPS1* and *ARG2* harbored putative quadruplex sequence (PQS) with a web-based server G4Hunter. Using standard parameters for the G4Hunter search algorithm (window size of 25 and G4HS $\geq$ 1.2), we identified four and six PQSs in *CPS1* and *ARG2* promoter, respectively (Figure 4A). Importantly, these potential G4s at the promoter of CPS1 and ARG2 do appear in the G4-seq human datasets previously published (Figure 4B), providing additional physical evidence to support our computational predictions. To investigate the influence of APE1 on the genome-wide distribution of G4s *in vivo*, we performed cleavage under targets and tagmentation (CUT&Tag) in *APE1*$^{+/+}$ and *APE1*$^{-/-}$ A549 and H1944 cells using BG4, a well-characterized

**Figure 3. APE1 is required to sustain *KRAS*$^{G12D}$-induced LUAD development in mice**

(A) Hematoxylin and eosin (H&E)-staining of tumor-bearing lungs from indicated genetically engineered mouse models (GEMMs). Lung tissues were collected at 17 weeks after Ad-CMV-Cre intranasal inhalation. Right panel showed the quantification of tumor burdens. For each mouse lung sample, the largest cross-section of the lung was selected as a representative for tumor quantification. $n$ = 7 tissue sections from seven mice. Scale bars indicate 2 mm. Statistical significance was assessed using two-tailed unpaired Student's t test.

(B) Scatterplot showing the DEGs in Ape1 knockout (left) or Ape1 N211A mutant (right) early-stage cancer cells versus *Ape1*$^{+/-}$ ones. Mice were intranasally administered with Ad-CMV-Cre. After 12 weeks, lungs were collected to sort tdTomato$^{+}$/EPCAM$^{+}$/DAPI$^{-}$/CD45$^{-}$/CD31$^{-}$ epithelial cells for RNA-seq analysis. $n$ = 4 mice for *Ape1*$^{+/-}$, *Kras*$^{G12D}$ genotype; $n$ = 3 mice for *Ape1*$^{-/-}$, *Kras*$^{G12D}$ or *Ape1*$^{N211A/-}$, *Kras*$^{G12D}$ genotype. nCount represents the mean of counts normalized by DESeq2. The dashed lines indicate the 2-fold change threshold for defining DEGs. Red and blue dots depict significantly changed genes (log2(fold change) $\geq$ 1 or $\leq$ −1 and $p$ value $\leq$0.05) and gray dots depict genes without significant changes. The number of DEGs is indicated.

(C and D) KEGG pathways analysis of DEGs in Ape1-deficient (C) or Ape1 N211A mutant (D) early-stage cancer cells. Pathways involved in amino acid biosynthesis and pyrimidine metabolism are indicated in red.

(E and F) Gene set enrichment analysis (GSEA) plots showing pathway involved in biosynthesis of amino acids in Ape1-deficient (E) or Ape1 N211A mutant (F) early-stage cancer cells. NES, normalized enrichment score.

(G) Representative immunohistochemistry (IHC) images for Arg2 in lung tumor tissues from indicated GEMMs. Lung tissues were collected at 17 weeks after Ad-CMVR-Cre infection. Scale bars indicate 200 μm (top) or 20 μm (bottom). All the data are presented as mean ± SEM.

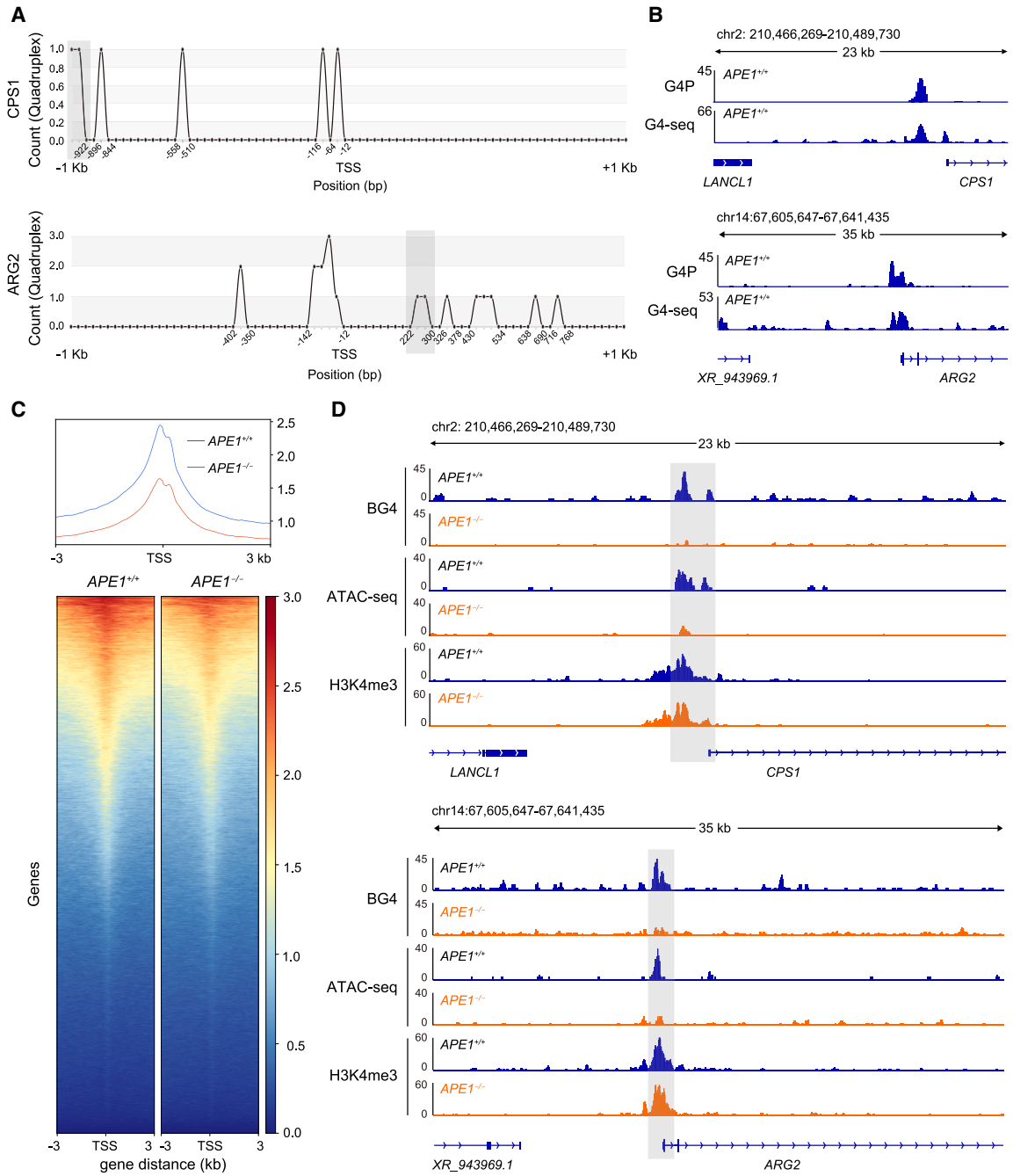


**Figure 4. APE1 knockout hinders the presence of G4 structures in the *CPS1* and *ARG2* promoters**

(A) Promoter sequences of *CPS1* (top) and *ARG2* (bottom) identified by G4Hunter using a window of 20 nucleotides and a threshold of 1.25 with their corresponding score on both forward and reverse strands. The shaded boxes indicate the G4-forming sequences used in Figure 5.

(B) Genome browser representation of G4 structures and Observed-G4s (OGs) at the promoters of *CPS1* (top) and *ARG2* (bottom) in human cells. Data of G4P ChIP-Seq and G4-seq are from GSE133379 and GSE63874, respectively.

(C) Reduced G4 signals in A549 cells upon APE1 deletion. Plot profile (top) and heatmaps (bottom) showing enrichment of G4 (RPGC, reads per genome coverage) in *APE1*$^{+/+}$ and *APE1*$^{-/-}$ A549 cells. The signal is plotted in a 6 kb window flanking the transcriptional start sites (TSS).

(D) Genome browser representation of G4 structures, H3K4me3 and chromatin accessibility at the promoters of *CPS1* (top) and *ARG2* (bottom). The shaded boxes highlight G4 structures co-occurring in the promoter regions enriched in H3K4me3.

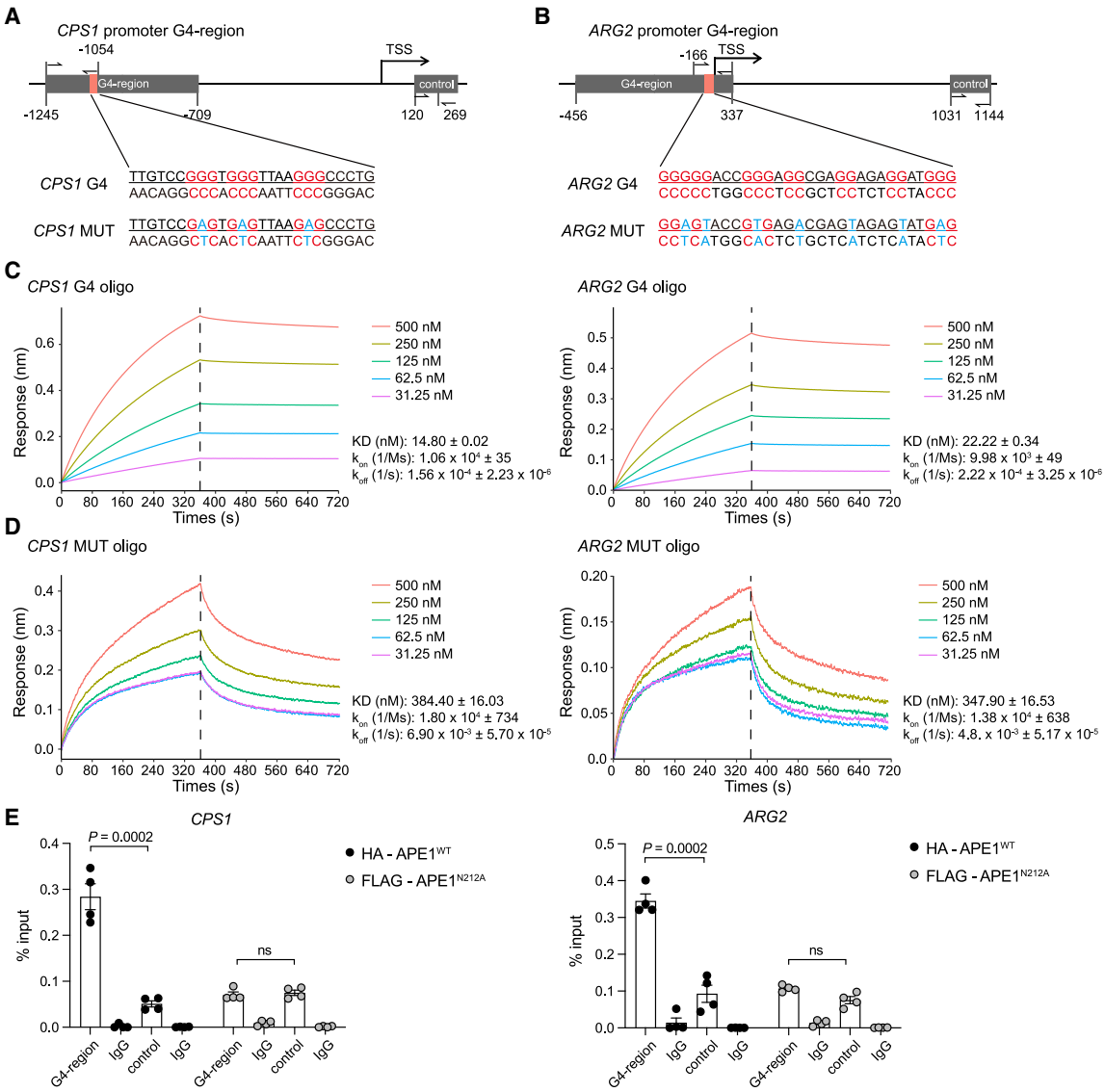


**Figure 5. APE1 shows strong binding affinity to G4 structures in CPS1 and ARG2 promoters**

(A and B) Schematic diagram of G4, non-G4 (control) regions and G4-mutated sequences at the *CPS1* (A) and *ARG2* (B) promoters. The underlined sequences denote G4-forming oligo containing the G4 motif or non-G4-forming oligo in which G residues are substituted with A (Mut, in blue). The location and length of each DNA fragment amplified in the real-time ChIP-PCR experiments (Figure 5E) are indicated. Arrows represent the positions of the primers. Red letters indicate the positions critical for G4 formation. TSS, transcription start site.

(C) Binding curves illustrating the association and dissociation of recombinant APE1 protein to the immobilized, biotinylated ssDNA oligonucleotide containing the *CPS1* (left) and *ARG2* (right) G4 by biolayer interferometry (BLI) analysis. Apparent KD for the most abundant population is indicated.

(D) BLI assay for non-G4-forming (MUT) oligonucleotides of *CPS1* (left) and *ARG2* (right).

(E) Enrichment of APE1 on the *CPS1* (left) and *ARG2* (right) promoters in knock-in A549 cells with HA-tagged APE1 (HA-APE1$^{WT}$) and in *APE1*$^{-/-}$ expressing transgenic FLAG-tagged APE1$^{N212A}$ (FLAG-APE1$^{N212A}$). ChIP-qPCR was performed, with control regions located within the gene body lacking G4-forming ability (Figure 5A). Data are presented as mean ± SEM from four biological replicates. Statistical significance was assessed using two-tailed unpaired Student's t test (E). ns, not significant.

G4-structure-specific scFv antibody. The metaplot displayed a reduction of G4 coverage in whole genome upon APE1 deletion (Figure 4C), suggesting the important role of APE1 in facilitating G4 formation *in vivo*. Consistent with previous studies,[37] we found that G4 structures were enriched in the promoters, 5′ untranslated regions (UTRs), and gene bodies (Figure S5B). To examine whether APE1 is involved in the formation of G4s in *CPS1* and *ARG2* promoter regions, we compared BG4 enrichment at these regions between *APE1*$^{+/+}$ and *APE1*$^{-/-}$ cells. A significant enrichment of G4 signals in *CPS1* and *ARG2* promoter regions was observed in *APE1*$^{+/+}$ A549 cells. However, this enrichment showed a striking decrease in *APE1*$^{-/-}$ A549

cells compared to WT cells (Figure 4D), with the same results observed in the H1944 cell line (Figure S5C). Additionally, our ATAC-seq data showed that there was significant reduction in the chromatin accessibility at the *CPS1* and *ARG2* loci following APE1 knockout (Figure 4D). However, no significant changes were detected in H3K4me3 levels. Taken together, our data indicate that APE1 is involved in G4-mediated transcription of *CPS1* and *ARG2*.

## APE1 shows strong binding affinity to G4 structures in *CPS1* and *ARG2* promoters

To validate the presence of G4 structures within the promoters of *CPS1* and *ARG2*, we synthesized a 25-mer oligonucleotide corresponding to the *CPS1* G4-proximal motif (named as *CPS1* G4 oligo) and a 29-mer oligonucleotide for *ARG2* (*ARG2* G4 oligo) (Figures 5A and 5B). Their mutants, designated as *CPS1* MUT oligo and *ARG2* MUT oligo, were generated to completely abrogate the formation of G4 structures (Figures 5A and 5B). G4 folding in the G4 oligonucleotides and their mutants was confirmed by circular dichroism spectroscopy (CD) and thermal difference UV/Vis spectroscopy (TDS). CD spectra confirmed that *CPS1* oligos formed parallel G4 structures, characterized by a strong positive ellipticity peak at 265 nm and a negative peak near 240 nm—typical signatures of G4 structures (Figure S6A). *ARG2* oligos formed antiparallel G4 structures, with a positive ellipticity band at 295 nm and a negative one at 260 nm (Figure S6A). TDS further confirmed the formation of G4 structures in both genes (Figures S6D and S6E). In contrast, CD and TDS analyses of the mutated *CPS1* and *ARG2* oligos, with several G residues replaced, showed a complete abrogation of G4 formation (Figures S6A–S6E). These findings indicate that the promoter regions of *CPS1* and *ARG2* can indeed form G4 structures *in vitro*.

To investigate the direct interaction between APE1 and G4 structures *in vitro*, we used bio-layer interferometry (BLI) to monitor real-time binding of APE1 to biotin-labeled *CPS1* and *ARG2* G4 oligonucleotides. APE1 showed selective binding to single-stranded *CPS1* G4 ($K_D$ = 14.80 nM) and *ARG2* G4 ($K_D$ = 22.22 nM) (Figure 5C), with negligible binding to the corresponding duplex DNA (Figure S6F) and over fifteen times weaker binding to single-stranded MUT oligos (Figure 5D). To further confirm APE1's direct binding to the G4 regions in the promoters of *CPS1* and *ARG2*, we performed chromatin immunoprecipitation assays followed by quantitative PCR (ChIP-qPCR) in A549 cells expressing C-terminally HA-tagged WT APE1 using HA antibodies (Figures S7A and S7B). WT APE1 directly bound to the G4 regions of *CPS1* and *ARG2*, while the catalytically inactive N212A mutant showed no promoter binding (Figure 5E). These findings demonstrate that APE1 selectively binds to G4 structures in the *CPS1* and *ARG2* promoters, and this interaction is dependent on its enzymatic activity.

## G4 structure positively regulates transcription of urea cycle enzymes

We next explore how APE1 loss reduces expression of *CPS1* and *ARG2*. Using CRISPR-Cas9 system,[38] we targeted G4-forming sequences within the endogenous *CPS1* and *ARG2* locus in A549 cells (Figure S7D). The first approach involved mutating these G4 sequences in A549 cells (validated previously as MUT oligos) to disrupt G4 structure formation, referred to as $CPS1^{MUT}$ and $ARG2^{MUT}$ (Figures 5A and 5B). G4 CUT&Tag with BG4 showed a drop of G4 signal in the $CPS1^{MUT}$ and $ARG2^{MUT}$ cells compared to $APE1^{+/+}$ cells (Figure 6A). Notably, RT-qPCR revealed a significant reduction in RNA levels for both genes (Figure 6B).

To evaluate whether the sequence itself or G4 structure is important for transcription, we then replaced the mutated *CPS1* and *ARG2* G4 motif with a well-characterized G4 sequence from the *MYC* locus (Figure S7E).[39] As previously reported,[31] APE1 exhibits high affinity for the *MYC* G4 ($K_D$ = 10.01 nM, Figures S7F and S7G). Remarkably, after replacing the *CPS1* and *ARG2* G4 regions with the *MYC* G4 sequence, their expression levels were restored to those in wild-type cells (Figure 6C). Overall, these results indicate that a folded G4 structure, rather than the specific sequence, promotes *CPS1* and *ARG2* expression through APE1 binding.

## APE1-dependent G4 structure and AP site formation drive *CPS1* and *ARG2* transcriptional regulation

We further confirmed the crucial role of APE1 in the formation of G4 structures using G4-stabilizing ligand pyridostatin (PDS). Upon treatment with PDS, we observed a significant upregulation of *CPS1* and *ARG2* expression in WT A549 cells, with no effect on *KRAS* expression (Figures 6D and S7H). Conversely, the same treatment in the $APE1^{-/-}$ cells failed to increase *CPS1* and *ARG2* expression (Figure 6D). Additionally, ectopically expression of WT APE1, but not the catalytically inactive N212A mutant, restored *CPS1* and *ARG2* expression in $APE1^{-/-}$ cells (Figure 6E), again without affecting *KRAS* levels (Figure S7I). Taken together, these results highlight the role of APE1 in regulating *CPS1* and *ARG2* expression via G4 structures.

To further explore the mechanism behind this regulation, we examined whether AP site formation by 8-oxoguanine DNA glycosylase 1 (OGG1) is essential for G4-mediated transcriptional control of CPS1 and ARG2. Treatment with a well-characterized OGG1 inhibitor TH5487 reduced *CPS1* and *ARG2* expression in WT but not $APE1^{-/-}$ cells (Figure 6F). Additionally, TH5487 inhibited the proliferation of WT cells but had no effect on $APE1^{-/-}$ cells, reinforcing the notion that APE1 is crucial for regulating the urea cycle and cell growth (Figure 6G). These observations aligned with previous findings that absence of OGG1 abolished the formation of most genomic G4s in cells,[32] suggesting the OGG1 inhibitor as a potential drug for LUAD. Together, these findings demonstrate that AP sites may be important for APE1-mediated transcriptional regulation of *CPS1* and *ARG2*.

## DISCUSSION

APE1 is a versatile protein with functions in DNA damage repair[21] and transcriptional regulation.[26] Mounting evidence shows the elevated expression of APE1 in various cancers and its correlation with malignancy, making it a promising prognostic cancer biomarker and a potential therapeutic target. Inhibition of APE1 induces DNA damage, apoptosis, pyroptosis, and necroptosis,

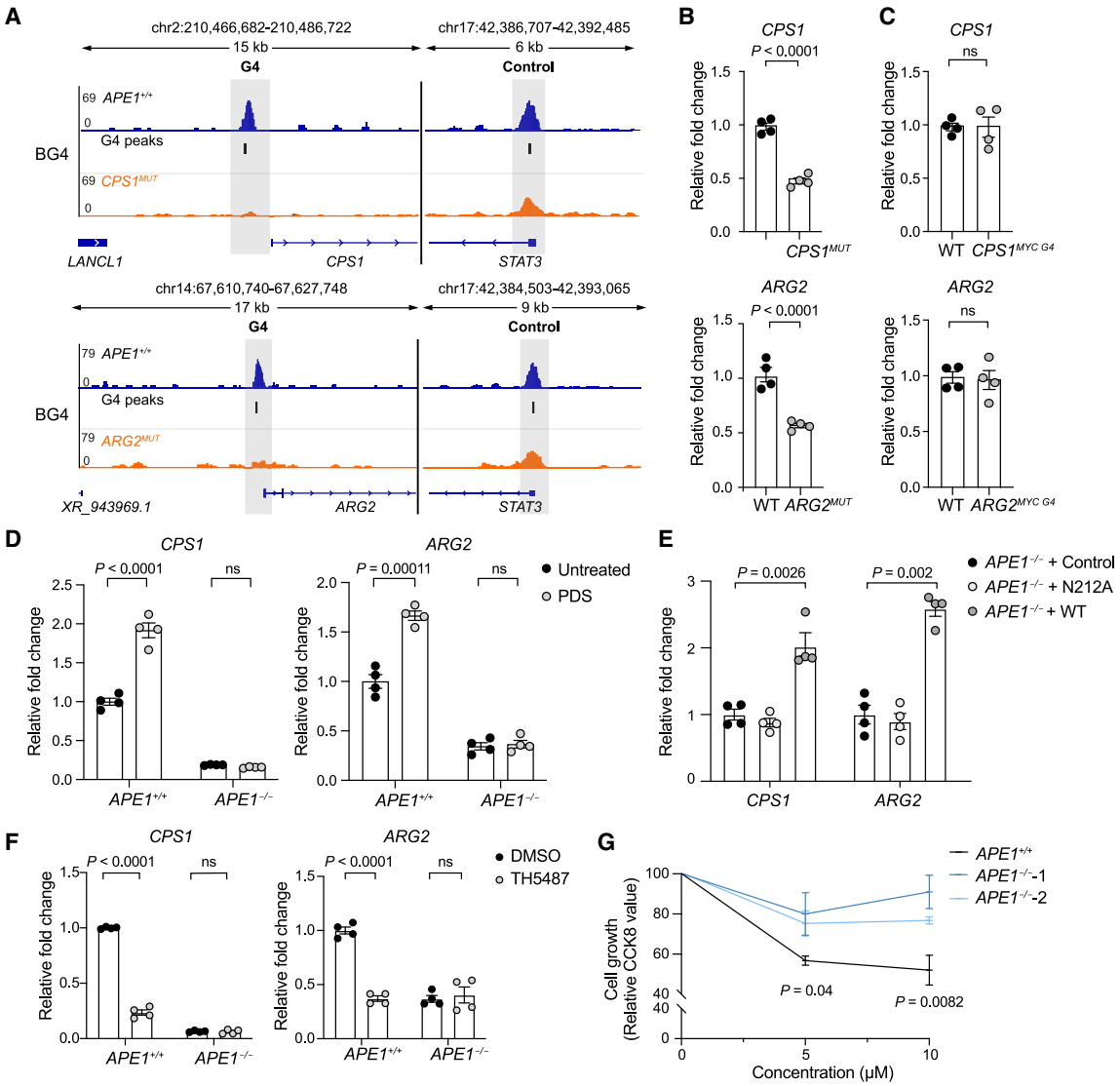


**Figure 6. APE1 regulates the transcription of *CPS1* and *ARG2* by facilitating G4 structure formation**

(A) BG4 CUT&Tag sequencing profiles for the G4 edited sites at the promoters of *CPS1* (upper) or *ARG2* (bottom) and the *STAT3* control site.

(B) RT-qPCR analysis of *CPS1* in $CPS1^{MUT}$ (top) and *ARG2* in $ARG2^{MUT}$ (bottom) A549 cells. "MUT" denotes that the G4 sequence in the promoter of the respective genes was mutated by gene editing.

(C) RT-qPCR analysis of *CPS1* in $CPS1^{MYC\ G4}$ (top) and *ARG2* in $ARG2^{MYC\ G4}$ (bottom) A549 cells. "MYC G4" denotes that the native G4 sequence in the promoter of the respective genes was replaced by *MYC* G4 sequence.

(D) RT-qPCR analysis of *CPS1* and *ARG2* in $APE1^{+/+}$ and $APE1^{-/-}$ A549 cells treated with G4-stabilizing ligand PDS (5 mM) for 2 h.

(E) RT-qPCR analysis of *CPS1* and *ARG2* in $APE1^{-/-}$ A549 cells with restoration of either APE1 WT or N212A mutant.

(F) RT-qPCR analysis of *CPS1* and *ARG2* in $APE1^{+/+}$ and $APE1^{-/-}$ A549 cells treated with OGG1 inhibitor TH5487 (5 μM) for 2 h.

(G) The proliferation of $APE1^{+/+}$ and $APE1^{-/-}$ A549 cells treated with OGG1 inhibitor TH5487 for 24 h. Cells were counted using the CCK8 assay. The expression levels were normalized to *GAPDH*, and then compared to the untreated $APE1^{+/+}$ control, which was set to 1.0.

Data in (B–G) are presented as mean ± SEM from three (G) or four (B–F) biological replicates. The data presented in (B–D) and (F and G) are derived from four independent CRISPR clones. Statistical significance was assessed using two-tailed unpaired Student's t test. ns, not significant.

thereby effectively inhibiting tumor growth.[40,41] However, the precise mechanism underlying how APE1 deletion inhibits tumor growth remains unclear.

The most striking finding of our study is the discovery of APE1's role in the activation of urea cycle genes through modulating the presence of G4 structures. As illustrated in graphical abstract, APE1 binds to AP sites generated by OGG1, facilitating the formation of G4 structures at the promoters of *CPS1* and *ARG2*. This ensures proper transcription of these urea cycle genes, which are essential for tumor progression. Correspondingly, APE1 deletion disrupts this process, leading to reprogramming of urea cycle metabolism, characterized by ammonia

accumulation and an imbalance in amino acid biosynthesis and pyrimidine metabolism.

G-quadruplex, a noncanonical tetrahelical nucleic acid structure that arises from the self-stacking of two or more guanine quartets into a planar array of four guanine residues coordinated through Hoogsteen hydrogen bonding.[42,43] While G4 structures have been recognized as an epigenetic mechanism involved in the transcriptional inhibition of various oncogenes, including *MYC*,[44] *VEGF*,[45] *BCL2*,[46] and *KIT*,[47] we find that by modulating the presence of G4 structures, APE1 promotes the expression of CPS1 and ARG2 in LUAD. Deletion of APE1 or removal of the G4-forming sequences on their promoters significantly reduces their transcription levels. This presents new evidence for G4's role in transcription activation.

It is worth mentioning that the cell lines and mouse model used in our study are KRAS mutant-driven models. Previous studies have demonstrated the role of APE1 in regulating stable G4 formation and *KRAS* expression in PDAC.[31,32] However, in our LUAD models, we observed that APE1 deletion had no effect on *KRAS* expression (Figures S1G and S1H), consistent with the findings from BG4 ChIP-seq data in GSE142284.[31] Additionally, treatment with PDS did not affect *KRAS* expression either (Figure S6D). Recent studies have showed that G4s appear to form under certain conditions, such as in response to specific stress stimuli, during specific stages of the cell cycle, or in a cell type-specific manner.[48,49] It remains possible that the discrepancy between these results may arise from the diverse regulation of *KRAS* in different tumor models. Understanding the regulation of G4 formation in a cellular context remains a fundamental and critical question for future investigations.

APE1 contains two major domains: a redox domain and a DNA repair domain, corresponding to its redox and endonuclease activities, respectively. Inhibitors targeting both activities have shown potential efficacy in cancer therapeutics.[50] Nevertheless, their molecular mechanisms for inhibiting tumor growth differ. Inhibition of the redox function prevents the cancer-associated TFs from being activated and subsequently affects the transcriptome. In contrast, our study reveals that APE1 regulates tumor progression through G4-mediated transcriptional regulation of urea cycle genes in an AP endonuclease activity dependent manner. The catalytically inactive N211A mutant phenocopies APE1 knockout in the mouse LUAD model, characterized by dysregulated urea cycles. Furthermore, overexpression of the N212A mutant in APE1 KO cells fails to upregulate CPS1 and ARG2, further highlighting the critical role of APE1's enzymatic activity in tumor growth through its regulation of the urea cycle.

Considering the elevated expression of APE1 in LUAD patients and its correlation with poor prognosis, APE1 has been identified as a potential target for cancer therapy. While several APE1 inhibitors have been developed, only APX3330 has successfully completed the phase 1 clinical trials. So far, no drug has reached the market due to unfavorable drug-like properties or lack of success in *in vivo* studies.[51] What's more, the limited specificity and considerable cytotoxicity of APE1 inhibitors have discouraged us from conducting experiments involving these inhibitors. Therefore, it is crucial to identify specific scenarios where APE1 inhibitors can be effectively utilized or explore alternative strategies, such as targeting metabolic pathway regulators or exploiting synthetic lethal effects with APE1, to enhance treatment response. Several studies have demonstrated that APE1 and CPS1 contribute to resistance against radiation and platinum-based chemotherapy.[52,53] Therefore, targeting APE1 and CPS1 with inhibitors in combination may hold promise as a therapeutic strategy. Additionally, our findings have suggested a negative correlation between ARG2 expression and disease-free survival in LUAD patients with high APE1 expression (Figure S8). LUAD cell lines with elevated ARG2 expression have showed heightened sensitivity to APE1 inhibitors (data not shown), also presenting a potential therapeutic opportunity for these patients.

In summary, our study has uncovered a novel mechanism by which APE1 promotes tumor progression through transcriptional reprogramming of urea cycle metabolism by modulating the presence of G4 structures. This adds another layer of complexity to the functions of APE1 and opens up avenues for further exploration to understand its role in diseases and explore potential therapeutic interventions. Targeting CPS1, ARG2, or related components may hold promise for LUAD patients with elevated APE1 expression.

## Limitations of the study

This study unveils the pivotal role of APE1 in LUAD, providing crucial insights for potential therapeutic interventions, yet it has several limitations. Primarily, the research is focused on *KRAS*-mutant LUAD models, raising questions about the applicability of our findings to LUAD with different genetic profiles or other cancer types. Expanding this research to include a diverse range of genetic backgrounds in LUAD and other malignancies is crucial for broader applicability. Furthermore, while we have elucidated APE1's involvement in regulating CPS1 and ARG2 expression via G4 structure formation, the detailed molecular mechanisms and the specific transcription factors interacting with APE1 in this pathway remain to be fully explored. Additionally, the low abundance and unique biological properties of APE1 present technical challenges for CUT&Tag experiments, limiting our ability to fully characterize its chromatin binding and highlighting the need for further methodological refinement. Another key aspect that requires attention is the translation of these findings into clinical practice. Although our results lay a promising groundwork, the clinical efficacy and safety of targeting APE1 and its associated pathways in human lung cancer remain to be validated. This necessitates rigorous clinical trials and translational research to establish whether interventions targeting APE1 can be a viable and safe therapeutic approach for LUAD patients.

## RESOURCE AVAILABILITY

### Lead contact

Further information and requests should be directed to the lead contact, Yarui Du (yrdu@sibcb.ac.cn).

### Materials availability

This study did not generate new unique materials.

### Data and code availability

- The RNA-seq data can be accessed through NCBI: GSE245168 and GSE245172.
- The CUT&Tag data can be accessed through NCBI: GSE245167.
- The ATAC-seq data can be accessed through NCBI: GSE271726.

- This article does not report original code.
- Other data will be made available upon reasonable request by the lead contact.

## ACKNOWLEDGMENTS

This study was supported by grants from National Natural Science Foundation of China (32370632 to Y.D. and 82088101 and 31991163 to G.X.), the Ministry of Science and Technology of the People's Republic of China (2019YFA0109900 to Y.D. and 2018YFA0800302 to G.X.), Shanghai Municipal Science and Technology Major Project (to G.X.), and the Sino-German Mobility Program (M-0313 to G.X.).

We thank Zhenfei Li, Jinchuan Hu and Xin Liu for fruitful discussions. We also thank Aibin He at the College of Future Technology, Institute of Molecular Medicine, Peking University for the assistance in ChIP-seq library preparation. We acknowledge the use of Biorender that is used to create the graphical abstract.

## AUTHOR CONTRIBUTIONS

G.X. conceived the original idea and, together with Y.D. Y.Y. and C.C. designed the experiments. C.C. contributed to the knockout/knockin design. C.C. and M.S. carried out CRISPR-Cas9 editing, mouse modeling. Y.Y., C.C. and Y.W. performed phenotyping, biochemistry, qPCR, ChIP-qPCR. Y.Y. carried out CUT&Tag library building and analysis. Y.Y. and Chaohan Wang carried out LC-MS sample preparation and analysis. Q.X. and Z.M. assisted for animal housing and genotyping. C.C. and Chao Wang performed SMART-Seq2 sample preparation and library building. Z.S. performed SMART-Seq2, RNA-seq analysis. Y.D. and Y.Y. wrote the paper, G.X., J.Z., D.Z., K.L. and H.J. revised the paper; all authors edited and approved the manuscript.

## DECLARATION OF INTERESTS

The authors declare no competing interests.

## STAR★METHODS

Detailed methods are provided in the online version of this paper and include the following:

- KEY RESOURCES TABLE
- EXPERIMENTAL MODEL AND STUDY PARTICIPANT DETAILS
  - Cells and cell culture
  - Mice and animal procedures
- METHOD DETAILS
  - Generation and validation of CRISPR-KO/KI cell lines
  - Cell viability assay
  - Cell-cycle analysis
  - RNA-seq library preparation
  - RNA-seq data analysis
  - Quantitative real-time PCR analysis
  - LC-MS sample preparation
  - LC-MS analysis
  - Fluorometric measurement of cellular ammonium content
  - Western blotting analysis
  - Generation of the Ape1 knockout and N211A mutant mice with CRISPR/Cas9-mediated gene editing technology
  - H&E staining, immunohistochemistry and immunofluorescence analysis
  - FACS analysis
  - ChIP–qPCR
  - Circular dichroism spectroscopy
  - Thermal difference spectra
  - Cleavage under targets and tagmentation (CUT&Tag)
  - ATAC-seq
  - Bio-layer interferometry assay
- QUANTIFICATION AND STATISTICAL ANALYSIS

## SUPPLEMENTAL INFORMATION

Supplemental information can be found online at https://doi.org/10.1016/j.isci.2025.112275.

Received: January 24, 2024
Revised: July 17, 2024
Accepted: March 19, 2025
Published: March 25, 2025

## REFERENCES

1. Wu, F., Wang, L., and Zhou, C. (2021). Lung cancer in China: current and prospect. Curr. Opin. Oncol. *33*, 40–46. https://doi.org/10.1097/CCO.0000000000000703.
2. Herbst, R.S., Morgensztern, D., and Boshoff, C. (2018). The biology and management of non-small cell lung cancer. Nature *553*, 446–454. https://doi.org/10.1038/nature25183.
3. Cancer Genome Atlas Research Network (2014). Comprehensive molecular profiling of lung adenocarcinoma. Nature *511*, 543–550. https://doi.org/10.1038/nature13385.
4. Cancer Genome Atlas Research Network Electronic address andrew_aguirre@dfci harvard edu; Cancer Genome Atlas Research Network (2017). Integrated Genomic Characterization of Pancreatic Ductal Adenocarcinoma. Cancer Cell *32*, 185–203.e13. https://doi.org/10.1016/j.ccell.2017.07.007.
5. La Montagna, M., Ginn, L., and Garofalo, M. (2021). Mechanisms of drug resistance mediated by long non-coding RNAs in non-small-cell lung cancer. Cancer Gene Ther. *28*, 175–187. https://doi.org/10.1038/s41417-020-00214-3.
6. Wang, M., Li, E., Lin, L., Kumar, A.K., Pan, F., He, L., Zhang, J., Hu, Z., and Guo, Z. (2019). Enhanced Activity of Variant DNA Polymerase beta (D160G) Contributes to Cisplatin Therapy by Impeding the Efficiency of NER. Mol. Cancer Res. *17*, 2077–2088. https://doi.org/10.1158/1541-7786.MCR-19-0482.
7. Li, L., Zhu, T., Gao, Y.F., Zheng, W., Wang, C.J., Xiao, L., Huang, M.S., Yin, J.Y., Zhou, H.H., and Liu, Z.Q. (2016). Targeting DNA Damage Response in the Radio(Chemo)therapy of Non-Small Cell Lung Cancer. Int. J. Mol. Sci. *17*, 839. https://doi.org/10.3390/ijms17060839.
8. Sak, S.C., Harnden, P., Johnston, C.F., Paul, A.B., and Kiltie, A.E. (2005). APE1 and XRCC1 protein expression levels predict cancer-specific survival following radical radiotherapy in bladder cancer. Clin. Cancer Res. *11*, 6205–6211. https://doi.org/10.1158/1078-0432.CCR-05-0045.
9. Puglisi, F., Aprile, G., Minisini, A.M., Barbone, F., Cataldi, P., Tell, G., Kelley, M.R., Damante, G., Beltrami, C.A., and Di Loreto, C. (2001). Prognostic significance of Ape1/ref-1 subcellular localization in non-small cell lung carcinomas. Anticancer Res. *21*, 4041–4049.
10. Yang, Z.Z., Li, M.X., Zhang, Y.S., Xiang, D.B., Dai, N., Zeng, L.L., Li, Z.P., Wang, G., and Wang, D. (2010). Knock down of the dual functional protein apurinic/apyrimidinic endonuclease 1 enhances the killing effect of hematoporphrphyrin derivative-mediated photodynamic therapy on non-small cell lung cancer cells in vitro and in a xenograft model. Cancer Sci. *101*, 180–187. https://doi.org/10.1111/j.1349-7006.2009.01366.x.
11. Bobola, M.S., Blank, A., Berger, M.S., Stevens, B.A., and Silber, J.R. (2001). Apurinic/apyrimidinic endonuclease activity is elevated in human adult gliomas. Clin. Cancer Res. *7*, 3510–3518.
12. Lau, J.P., Weatherdon, K.L., Skalski, V., and Hedley, D.W. (2004). Effects of gemcitabine on APE/ref-1 endonuclease activity in pancreatic cancer cells, and the therapeutic potential of antisense oligonucleotides. Br. J. Cancer *91*, 1166–1173. https://doi.org/10.1038/sj.bjc.6602080.
13. Fritz, G., Grösch, S., Tomicic, M., and Kaina, B. (2003). APE/Ref-1 and the mammalian response to genotoxic stress. Toxicology *193*, 67–78. https://doi.org/10.1016/s0300-483x(03)00290-7.

14. Kelley, M.R., Cheng, L., Foster, R., Tritt, R., Jiang, J., Broshears, J., and Koch, M. (2001). Elevated and altered expression of the multifunctional DNA base excision repair and redox enzyme Ape1/ref-1 in prostate cancer. Clin. Cancer Res. *7*, 824–830.

15. Freitas, S., Moore, D.H., Michael, H., and Kelley, M.R. (2003). Studies of apurinic/apyrimidinic endonuclease/ref-1 expression in epithelial ovarian cancer: correlations with tumor progression and platinum resistance. Clin. Cancer Res. *9*, 4689–4694.

16. Sultana, R., McNeill, D.R., Abbotts, R., Mohammed, M.Z., Zdzienicka, M.Z., Qutob, H., Seedhouse, C., Laughton, C.A., Fischer, P.M., Patel, P.M., et al. (2012). Synthetic lethal targeting of DNA double-strand break repair deficient cells by human apurinic/apyrimidinic endonuclease inhibitors. Int. J. Cancer *131*, 2433–2444. https://doi.org/10.1002/ijc.27512.

17. Wang, D., Xiang, D.B., Yang, X.Q., Chen, L.S., Li, M.X., Zhong, Z.Y., and Zhang, Y.S. (2009). APE1 overexpression is associated with cisplatin resistance in non-small cell lung cancer and targeted inhibition of APE1 enhances the activity of cisplatin in A549 cells. Lung Cancer *66*, 298–304. https://doi.org/10.1016/j.lungcan.2009.02.019.

18. Koukourakis, M.I., Giatromanolaki, A., Kakolyris, S., Sivridis, E., Georgoulias, V., Funtzilas, G., Hickson, I.D., Gatter, K.C., and Harris, A.L. (2001). Nuclear expression of human apurinic/apyrimidinic endonuclease (HAP1/Ref-1) in head-and-neck cancer is associated with resistance to chemoradiotherapy and poor outcome. Int. J. Radiat. Oncol. Biol. Phys. *50*, 27–36. https://doi.org/10.1016/s0360-3016(00)01561-3.

19. Wang, D., Luo, M., and Kelley, M.R. (2004). Human apurinic endonuclease 1 (APE1) expression and prognostic significance in osteosarcoma: enhanced sensitivity of osteosarcoma to DNA damaging agents using silencing RNA APE1 expression inhibition. Mol. Cancer Ther. *3*, 679–686.

20. Xiang, D.B., Chen, Z.T., Wang, D., Li, M.X., Xie, J.Y., Zhang, Y.S., Qing, Y., Li, Z.P., and Xie, J. (2008). Chimeric adenoviral vector Ad5/F35-mediated APE1 siRNA enhances sensitivity of human colorectal cancer cells to radiotherapy in vitro and in vivo. Cancer Gene Ther. *15*, 625–635. https://doi.org/10.1038/cgt.2008.30.

21. Demple, B., Herman, T., and Chen, D.S. (1991). Cloning and expression of APE, the cDNA encoding the major human apurinic endonuclease: definition of a family of DNA repair enzymes. Proc. Natl. Acad. Sci. USA *88*, 11450–11454. https://doi.org/10.1073/pnas.88.24.11450.

22. Demple, B., and Harrison, L. (1994). Repair of oxidative damage to DNA: enzymology and biology. Annu. Rev. Biochem. *63*, 915–948. https://doi.org/10.1146/annurev.bi.63.070194.004411.

23. Rothwell, D.G., and Hickson, I.D. (1996). Asparagine 212 is essential for abasic site recognition by the human DNA repair endonuclease HAP1. Nucleic Acids Res. *24*, 4217–4221. https://doi.org/10.1093/nar/24.21.4217.

24. Kanazhevskaya, L.Y., Koval, V.V., Lomzov, A.A., and Fedorova, O.S. (2014). The role of Asn-212 in the catalytic mechanism of human endonuclease APE1: stopped-flow kinetic study of incision activity on a natural AP site and a tetrahydrofuran analogue. DNA Repair *21*, 43–54. https://doi.org/10.1016/j.dnarep.2014.06.008.

25. Li, M., and Wilson, D.M., 3rd. (2014). Human apurinic/apyrimidinic endonuclease 1. Antioxid. Redox Signal. *20*, 678–707. https://doi.org/10.1089/ars.2013.5492.

26. Tell, G., Quadrifoglio, F., Tiribelli, C., and Kelley, M.R. (2009). The many functions of APE1/Ref-1: not only a DNA repair enzyme. Antioxid. Redox Signal. *11*, 601–620. https://doi.org/10.1089/ars.2008.2194.

27. Shah, F., Logsdon, D., Messmann, R.A., Fehrenbacher, J.C., Fishel, M.L., and Kelley, M.R. (2017). Exploiting the Ref-1-APE1 node in cancer signaling and other diseases: from bench to clinic. npj Precis. Oncol. *1*, 19. https://doi.org/10.1038/s41698-017-0023-0.

28. Logsdon, D.P., Grimard, M., Luo, M., Shahda, S., Jiang, Y., Tong, Y., Yu, Z., Zyromski, N., Schipani, E., Carta, F., et al. (2016). Regulation of HIF1alpha under Hypoxia by APE1/Ref-1 Impacts CA9 Expression: Dual Targeting in Patient-Derived 3D Pancreatic Cancer Models. Mol. Cancer Ther. *15*, 2722–2732. https://doi.org/10.1158/1535-7163.MCT-16-0253.

29. Fishel, M.L., Jiang, Y., Rajeshkumar, N.V., Scandura, G., Sinn, A.L., He, Y., Shen, C., Jones, D.R., Pollok, K.E., Ivan, M., et al. (2011). Impact of APE1/Ref-1 redox inhibition on pancreatic tumor growth. Mol. Cancer Ther. *10*, 1698–1708. https://doi.org/10.1158/1535-7163.MCT-11-0107.

30. Walker, L.J., Robson, C.N., Black, E., Gillespie, D., and Hickson, I.D. (1993). Identification of residues in the human DNA repair enzyme HAP1 (Ref-1) that are essential for redox regulation of Jun DNA binding. Mol. Cell Biol. *13*, 5370–5376. https://doi.org/10.1128/mcb.13.9.5370-5376.1993.

31. Roychoudhury, S., Pramanik, S., Harris, H.L., Tarpley, M., Sarkar, A., Spagnol, G., Sorgen, P.L., Chowdhury, D., Band, V., Klinkebiel, D., and Bhakat, K.K. (2020). Endogenous oxidized DNA bases and APE1 regulate the formation of G-quadruplex structures in the genome. Proc. Natl. Acad. Sci. USA *117*, 11409–11420. https://doi.org/10.1073/pnas.1912355117.

32. Pramanik, S., Chen, Y., Song, H., Khutsishvili, I., Marky, L.A., Ray, S., Natarajan, A., Singh, P.K., and Bhakat, K.K. (2022). The human AP-endonuclease 1 (APE1) is a DNA G-quadruplex structure binding protein and regulates KRAS expression in pancreatic ductal adenocarcinoma cells. Nucleic Acids Res. *50*, 3394–3412. https://doi.org/10.1093/nar/gkac172.

33. Wei, X., Li, Q., Li, Y., Duan, W., Huang, C., Zheng, X., Sun, L., Luo, J., Wang, D., Zhang, S., et al. (2016). Prediction of survival prognosis of non-small cell lung cancer by APE1 through regulation of Epithelial-Mesenchymal Transition. Oncotarget *7*, 28523–28539. https://doi.org/10.18632/oncotarget.8660.

34. Xu, Q., Wang, C., Zhou, J.X., Xu, Z.M., Gao, J., Sui, P., Walsh, C.P., Ji, H., and Xu, G.L. (2022). Loss of TET reprograms Wnt signaling through impaired demethylation to promote lung cancer development. Proc. Natl. Acad. Sci. USA *119*, e2107599119. https://doi.org/10.1073/pnas.2107599119.

35. Martinez-Reyes, I., and Chandel, N.S. (2021). Cancer metabolism: looking forward. Nat. Rev. Cancer *21*, 669–680. https://doi.org/10.1038/s41568-021-00378-6.

36. Kim, J., Hu, Z., Cai, L., Li, K., Choi, E., Faubert, B., Bezwada, D., Rodriguez-Canales, J., Villalobos, P., Lin, Y.F., et al. (2017). CPS1 maintains pyrimidine pools and DNA synthesis in KRAS/LKB1-mutant lung cancer cells. Nature *546*, 168–172. https://doi.org/10.1038/nature22359.

37. Hansel-Hertsch, R., Beraldi, D., Lensing, S.V., Marsico, G., Zyner, K., Parry, A., Di Antonio, M., Pike, J., Kimura, H., Narita, M., et al. (2016). G-quadruplex structures mark human regulatory chromatin. Nat. Genet. *48*, 1267–1272. https://doi.org/10.1038/ng.3662.

38. Jinek, M., Chylinski, K., Fonfara, I., Hauer, M., Doudna, J.A., and Charpentier, E. (2012). A programmable dual-RNA-guided DNA endonuclease in adaptive bacterial immunity. Science *337*, 816–821. https://doi.org/10.1126/science.1225829.

39. Esain-Garcia, I., Kirchner, A., Melidis, L., Tavares, R.d.C.A., Dhir, S., Simeone, A., Yu, Z., Madden, S.K., Hermann, R., Tannahill, D., and Balasubramanian, S. (2024). G-quadruplex DNA structure is a positive regulator of MYC transcription. Proc. Natl. Acad. Sci. USA *121*, e2320240121. https://doi.org/10.1073/pnas.2320240121.

40. Long, K., Gu, L., Li, L., Zhang, Z., Li, E., Zhang, Y., He, L., Pan, F., Guo, Z., and Hu, Z. (2021). Small-molecule inhibition of APE1 induces apoptosis, pyroptosis, and necroptosis in non-small cell lung cancer. Cell Death Dis. *12*, 503. https://doi.org/10.1038/s41419-021-03804-7.

41. Sun, Z., Zhu, Y., Zhang, N., Fan, Q., Fan, Q., and Peng, J. (2018). Differential expression of APE1 in hepatocellular carcinoma and the effects on proliferation and apoptosis of cancer cells. Biosci. Trends *12*, 456–462. https://doi.org/10.5582/bst.2018.01239.

42. Bochman, M.L., Paeschke, K., and Zakian, V.A. (2012). DNA secondary structures: stability and function of G-quadruplex structures. Nat. Rev. Genet. *13*, 770–780. https://doi.org/10.1038/nrg3296.

43. Gellert, M., Lipsett, M.N., and Davies, D.R. (1962). Helix formation by guanylic acid. Proc. Natl. Acad. Sci. USA *48*, 2013–2018. https://doi.org/10.1073/pnas.48.12.2013.

44. Siddiqui-Jain, A., Grand, C.L., Bearss, D.J., and Hurley, L.H. (2002). Direct evidence for a G-quadruplex in a promoter region and its targeting with a small molecule to repress c-MYC transcription. Proc. Natl. Acad. Sci. USA *99*, 11593–11598. https://doi.org/10.1073/pnas.182256799.

45. Sun, D., Guo, K., Rusche, J.J., and Hurley, L.H. (2005). Facilitation of a structural transition in the polypurine/polypyrimidine tract within the proximal promoter region of the human VEGF gene by the presence of potassium and G-quadruplex-interactive agents. Nucleic Acids Res. *33*, 6070–6080. https://doi.org/10.1093/nar/gki917.

46. Dexheimer, T.S., Sun, D., and Hurley, L.H. (2006). Deconvoluting the structural and drug-recognition complexity of the G-quadruplex-forming region upstream of the bcl-2 P1 promoter. J. Am. Chem. Soc. *128*, 5404–5415. https://doi.org/10.1021/ja0563861.

47. Rankin, S., Reszka, A.P., Huppert, J., Zloh, M., Parkinson, G.N., Todd, A.K., Ladame, S., Balasubramanian, S., and Neidle, S. (2005). Putative DNA quadruplex formation within the human c-kit oncogene. J. Am. Chem. Soc. *127*, 10584–10589. https://doi.org/10.1021/ja050823u.

48. Spiegel, J., Adhikari, S., and Balasubramanian, S. (2020). The Structure and Function of DNA G-Quadruplexes. Trends Chem. *2*, 123–136. https://doi.org/10.1016/j.trechm.2019.07.002.

49. Varshney, D., Spiegel, J., Zyner, K., Tannahill, D., and Balasubramanian, S. (2020). The regulation and functions of DNA and RNA G-quadruplexes. Nat. Rev. Mol. Cell Biol. *21*, 459–474. https://doi.org/10.1038/s41580-020-0236-x.

50. Caston, R.A., Gampala, S., Armstrong, L., Messmann, R.A., Fishel, M.L., and Kelley, M.R. (2021). The multifunctional APE1 DNA repair-redox signaling protein as a drug target in human disease. Drug Discov. Today *26*, 218–228. https://doi.org/10.1016/j.drudis.2020.10.015.

51. Zhang, Z., Wu, Z., Shi, X., Guo, D., Cheng, Y., Gao, J., Liu, L., Liu, W., Liang, L., Peng, L., and Hu, J. (2022). Research Progress in Human AP Endonuclease 1: Structure, Catalytic Mechanism, and Inhibitors. Curr. Protein Pept. Sci. *23*, 77–88. https://doi.org/10.2174/1389203723666220406132737.

52. Celiktas, M., Tanaka, I., Tripathi, S.C., Fahrmann, J.F., Aguilar-Bonavides, C., Villalobos, P., Delgado, O., Dhillon, D., Dennison, J.B., Ostrin, E.J., et al. (2017). Role of CPS1 in Cell Growth, Metabolism and Prognosis in LKB1-Inactivated Lung Adenocarcinoma. J Natl Cancer Inst *109*, 1–9. https://doi.org/10.1093/jnci/djw231.

53. Liu, Y., Zhang, Z., Li, Q., Zhang, L., Cheng, Y., and Zhong, Z. (2020). Mitochondrial APE1 promotes cisplatin resistance by downregulating ROS in osteosarcoma. Oncol. Rep. *44*, 499–508. https://doi.org/10.3892/or.2020.7633.

54. Langmead, B., and Salzberg, S.L. (2012). Fast gapped-read alignment with Bowtie 2. Nat. Methods *9*, 357–359. https://doi.org/10.1038/nmeth.1923.

55. Ramirez, F., Ryan, D.P., Gruning, B., Bhardwaj, V., Kilpert, F., Richter, A.S., Heyne, S., Dundar, F., and Manke, T. (2016). deepTools2: a next generation web server for deep-sequencing data analysis. Nucleic Acids Res. *44*, W160–W165. https://doi.org/10.1093/nar/gkw257.

56. Siren, J., Valimaki, N., and Makinen, V. (2014). Indexing Graphs for Path Queries with Applications in Genome Research. IEEE ACM Trans. Comput. Biol. Bioinf *11*, 375–388. https://doi.org/10.1109/TCBB.2013.2297101.

57. Liao, Y., Smyth, G.K., and Shi, W. (2019). The R package Rsubread is easier, faster, cheaper and better for alignment and quantification of RNA sequencing reads. Nucleic Acids Res. *47*, e47. https://doi.org/10.1093/nar/gkz114.

58. Sherman, B.T., Hao, M., Qiu, J., Jiao, X., Baseler, M.W., Lane, H.C., Imamichi, T., and Chang, W. (2022). DAVID: a web server for functional enrichment analysis and functional annotation of gene lists (2021 update). Nucleic Acids Res. *50*, W216–W221. https://doi.org/10.1093/nar/gkac194.

59. Xu, S., Hu, E., Cai, Y., Xie, Z., Luo, X., Zhan, L., Tang, W., Wang, Q., Liu, B., Wang, R., et al. (2024). Using clusterProfiler to characterize multiomics data. Nat. Protoc. *19*, 3292–3320. https://doi.org/10.1038/s41596-024-01020-z.

60. Jackson, E.L., Willis, N., Mercer, K., Bronson, R.T., Crowley, D., Montoya, R., Jacks, T., and Tuveson, D.A. (2001). Analysis of lung tumor initiation and progression using conditional expression of oncogenic K-ras. Genes Dev. *15*, 3243–3248. https://doi.org/10.1101/gad.943001.

61. Madisen, L., Zwingman, T.A., Sunkin, S.M., Oh, S.W., Zariwala, H.A., Gu, H., Ng, L.L., Palmiter, R.D., Hawrylycz, M.J., Jones, A.R., et al. (2010). A robust and high-throughput Cre reporting and characterization system for the whole mouse brain. Nat. Neurosci. *13*, 133–140. https://doi.org/10.1038/nn.2467.

62. Yang, H., Wang, H., and Jaenisch, R. (2014). Generating genetically modified mice using CRISPR/Cas-mediated genome engineering. Nat. Protoc. *9*, 1956–1968. https://doi.org/10.1038/nprot.2014.134.

63. Picelli, S., Björklund, Å.K., Faridani, O.R., Sagasser, S., Winberg, G., and Sandberg, R. (2013). Smart-seq2 for sensitive full-length transcriptome profiling in single cells. Nat. Methods *10*, 1096–1098. https://doi.org/10.1038/nmeth.2639.

64. Xue, J.H., Chen, G.D., Hao, F., Chen, H., Fang, Z., Chen, F.F., Pang, B., Yang, Q.L., Wei, X., Fan, Q.Q., et al. (2019). A vitamin-C-derived DNA modification catalysed by an algal TET homologue. Nature *569*, 581–585. https://doi.org/10.1038/s41586-019-1160-0.

65. Wang, H., Yang, H., Shivalila, C.S., Dawlaty, M.M., Cheng, A.W., Zhang, F., and Jaenisch, R. (2013). One-step generation of mice carrying mutations in multiple genes by CRISPR/Cas-mediated genome engineering. Cell *153*, 910–918. https://doi.org/10.1016/j.cell.2013.04.025.

66. Yang, H., Wang, H., Shivalila, C.S., Cheng, A.W., Shi, L., and Jaenisch, R. (2013). One-step generation of mice carrying reporter and conditional alleles by CRISPR/Cas-mediated genome engineering. Cell *154*, 1370–1379. https://doi.org/10.1016/j.cell.2013.08.022.

67. Dai, H.Q., Wang, B.A., Yang, L., Chen, J.J., Zhu, G.C., Sun, M.L., Ge, H., Wang, R., Chapman, D.L., Tang, F., et al. (2016). TET-mediated DNA demethylation controls gastrulation by regulating Lefty-Nodal signalling. Nature *538*, 528–532. https://doi.org/10.1038/nature20095.

68. Tammela, T., Sanchez-Rivera, F.J., Cetinbas, N.M., Wu, K., Joshi, N.S., Helenius, K., Park, Y., Azimi, R., Kerper, N.R., Wesselhoeft, R.A., et al. (2017). A Wnt-producing niche drives proliferative potential and progression in lung adenocarcinoma. Nature *545*, 355–359. https://doi.org/10.1038/nature22334.

69. Marjanovic, N.D., Hofree, M., Chan, J.E., Canner, D., Wu, K., Trakala, M., Hartmann, G.G., Smith, O.C., Kim, J.Y., Evans, K.V., et al. (2020). Emergence of a High-Plasticity Cell State during Lung Cancer Evolution. Cancer Cell *38*, 229–246.e13. https://doi.org/10.1016/j.ccell.2020.06.012.

70. LaFave, L.M., Kartha, V.K., Ma, S., Meli, K., Del Priore, I., Lareau, C., Naranjo, S., Westcott, P.M.K., Duarte, F.M., Sankar, V., et al. (2020). Epigenomic State Transitions Characterize Tumor Progression in Mouse Lung Adenocarcinoma. Cancer Cell *38*, 212–228.e13. https://doi.org/10.1016/j.ccell.2020.06.006.

71. Li, C., Wang, H., Yin, Z., Fang, P., Xiao, R., Xiang, Y., Wang, W., Li, Q., Huang, B., Huang, J., and Liang, K. (2021). Ligand-induced native G-quadruplex stabilization impairs transcription initiation. Genome Res. *31*, 1546–1560. https://doi.org/10.1101/gr.275431.121.

72. Buenrostro, J.D., Giresi, P.G., Zaba, L.C., Chang, H.Y., and Greenleaf, W.J. (2013). Transposition of native chromatin for fast and sensitive epigenomic profiling of open chromatin, DNA-binding proteins and nucleosome position. Nat. Methods *10*, 1213–1218. https://doi.org/10.1038/nmeth.2688.

## STAR★METHODS

### KEY RESOURCES TABLE

| REAGENT or RESOURCE | SOURCE | IDENTIFIER |
|---|---|---|
| Antibodies | | |
| anti-APE1 | Abcam | Cat# ab194; RRID: AB_302694 |
| anti-CPS1 | ABclonal | Cat# A4214; RRID: AB_2863210 |
| anti-HA | Cell Signalling Technology | Cat# 3724; RRID: 9 |
| anti-FLAG | Sigma-Aldrich | Cat# F1804; RRID: AB_262044 |
| anti-KRAS | Sigma-Aldrich | Cat# WH0003845M1; RRID: AB_1842235 |
| anti-ARG2 | Cell Signalling Technology | Cat# 55003; RRID: D951N |
| anti-β-actin | ABclonal | Cat# AC026; RRID: AB_2768234 |
| HRP conjugated goat anti-mouse IgG | Jackson | Cat# 115-035-003; RRID: 116816 |
| goat anti-rabbit IgG | Jackson | Cat# 111-035-003; RRID: 118822 |
| anti-Phospho-Histone H2A.X (Ser139) (20E3) | Cell Signalling Technology | Cat# 9718; RRID: AB_2118009 |
| Cy3 goat anti-rabbit IgG | Jackson ImmunoResearch | Cat# 111-165-144; RRID: AB_2338006 |
| anti-CD45 APC | BioLegend | Cat# 103112; RRID: B363792 |
| anti-CD31 APC | BioLegend | Cat# 102510; RRID: B417515 |
| anti-CD326 (EPCAM) APC/Cy7 | BioLegend | Cat# 118218; RRID: B393333 |
| DAPI | BBI | Cat# E607303; RRID: J214FA0002 |
| anti-H3K4me3 | Abcam | Cat# ab8580; RRID: 1083744-1 |
| Bacterial and virus strains | | |
| Trans5α Chemically Competent Cell | Trans-gene | Cat# CD201-01 |
| Chemicals, peptides, and recombinant proteins | | |
| DMEM medium | Gibco | Cat# 11965118; RRID: 2902921 |
| Fetal Bovine Serum (FBS) | ExCell | Cat# FSP500; RRID: 12B259 |
| RPMI1640 | Gibco | Cat# 11875119; RRID: 2902871 |
| 0.25% Trypsin-EDTA | Gibco | Cat# 25200056; RRID: 2764719 |
| sodium pyruvate | Gibco | Cat# 11360070; RRID: 2813888 |
| penicillin and streptomycin | Gibco | Cat# 15140122; RRID: 227766 |
| Dextran sodium sulfate (SDS) | Diamond | Cat# A100227; RRID: H706BA0008 |
| HEPES pH 7.3 | ABCONE | Cat# H33755; RRID: AOB101941 |
| Tween 20 | Diamand | Cat# A100777; RRID: G309BA0013 |
| EDTA pH8.0 | Sigma-Aldrich | Cat# E6758; RRID: WXBD5250V |
| Tris-base | ABCONE | Cat# T15033; RRID: AOB101975 |
| KCl | Shanghai Experiment Reagent Co., Ltd | Cat# 167690; RRID: 20220309 |
| NaCl | Hushi Laboratorial Co., Ltd | Cat# 10019318; RRID: 20240119 |
| LiCl | Hushi Laboratorial Co., Ltd | Cat# 80074718; RRID: 20230112 |
| MgCl | Sinopharm Chemical Reagent Co., Ltd | Cat# 7791-18-6; RRID: 20150921 |
| Igepal CA-630 | Sigma-Aldrich | Cat# I8896; RRID: MKCD3510 |
| LiCacodylate | Sigma-Aldrich | Cat# 20835; RRID: BCC52636 |
| Uridine | Sigma-Aldrich | Cat# U3003; RRID: BCCD9057 |
| thymidine | Sigma-Aldrich | Cat# T1895; RRID: WXBD8981V |
| adenosine | Sigma-Aldrich | Cat# A4036; RRID: SLCP3777 |
| G4-ligand PDS | MCE | Cat# HY-15176A; RRID: 84340 |
| TH5487 | MCE | Cat# HY-125276; RRID: 50214 |
| purified human APE1 protein | Cytosinlab Therapeutics | N/A |

(*Continued on next page*)

*Continued*

| REAGENT or RESOURCE | SOURCE | IDENTIFIER |
|---|---|---|
| **Critical commercial assays** | | |
| Cell Counting Kit 8 | Dojindo | Cat# CK04 |
| SuperPico ECL Chemiluminescence Kit | Vazyme | Cat# E422 |
| Pharmingen™ FITC BrdU Flow Kit | BD | Cat# 559619 |
| VAHTS mRNA-seq V3 Library Prep Kit for Illumina | Vazyme | Cat# NR611 |
| TruePrep DNA Library Prep Kit V2 for Illumina | Vazyme | Cat# TD503 |
| PrimeScript RT reagent Kit | Takara | Cat# RR047A |
| ammonium assay kit | Sigma-Aldrich | Cat# MAK310 |
| ProteinExt Mammalian Total Protein Extraction Kit | Transgen | Cat# DE101 |
| Hyperactive Universal CUT&Tag Assay Kit protocol | Vazyme | Cat# TD904 |
| **Deposited data** | | |
| Raw and analyzed data | This paper | GEO: GSE245168, GSE245172, GSE245167, GSE271726 |
| Human reference genome NCBI build 38, GRCh38 | Genome Reference Consortium | https://www.ncbi.nlm.nih.gov/grc/human |
| Mouse reference genome NCBI build 38, GRCm38 | Genome Reference Consortium | https://www.ncbi.nlm.nih.gov/grc/mouse |
| BG4 ChIP-seq data | Genome-wide mapping of AP sites, binding of repair proteins and G4 structure formation | GEO: GSE142284 |
| RNA-seq in WT and shAPE1 A549 cells | Genome-wide mapping of AP sites, binding of repair proteins and G4 structure formation | GEO: GSE142284 |
| G4P ChIP-Seq | Detection of genomic G-quadruplexes in living cells using a small artificial protein | GEO: GSE133379 |
| Observed-G4s (OGs)-seq | High-throughput sequencing of DNA G-quadruplex structures in the human genome | GEO: GSE63874 |
| RNA-seq (Figures 2A, 3B–3F and S2A–S2D) | This paper | GEO: GSE245168 and GSE245172 |
| BG4 CUT&Tag (Figures 4C, 4D, 6A, S5B and S5C) | This paper | GEO: GSE245167 |
| ATAC-seq (Figure 4D) | This paper | GEO: GSE271726 |
| **Experimental models: Cell lines** | | |
| A549 | National Collection of Authenticated Cell Cultures | Cat# SCSP-503; CSTR: 19375.09.3101HUMSCSP503 |
| NCI-H1944 | National Collection of Authenticated Cell Cultures | Cat# SCSP-596; CSTR: 19375.09.3101HUMSCSP596 |
| 293T | National Collection of Authenticated Cell Cultures | Cat# SCSP-502; CSTR: 19375.09.3101HUMSCSP502 |
| **Experimental models: Organisms/strains** | | |
| *Kras* $^{LSL\text{-}G12D/+}$ mice | Jackson Laboratory [JAX] | stock No. 008179 |
| *Rosa26* $^{LSL\text{-}tdTomato/+}$ mice | Jackson Laboratory [JAX] | stock No. 007909 |
| **Oligonucleotides** | | |
| sgRNA for editing APE1 using CRISPR/Cas9, see Table S1 | This paper | N/A |
| Primers for qPCR and ChIP-qPCR, see Table S2 | This paper | N/A |

(*Continued on next page*)

*Continued*

| REAGENT or RESOURCE | SOURCE | IDENTIFIER |
|---|---|---|
| Oligonucleotides for CD, TDS and BLI, see Methods | This paper | N/A |
| **Recombinant DNA** | | |
| pX330-U6-Chimeric-BB-CBh-hSpCas9 | Howard Hughes Medical Institute | Laboratory of Feng Zhang |
| pCDH-CMV-MCS-EF1-copGFP | Center for Excellence in Molecular Cell Science | Laboratory of Hongbin Ji |
| pCDH-CMV-3xflag-MCS-EF1-Cre | Center for Excellence in Molecular Cell Science | Laboratory of Hongbin Ji |
| pLVX-2Flag-MCS-IRES-mCherry | Fudan University | Laboratory of Zhigang Lu |
| **Software and algorithms** | | |
| FlowJo v10.0.7 | Leonard Herzenberg | https://www.flowjo.com/ |
| Bowtie2 v2.3.1 | Langmead and Salzberg[54] | https://bowtie-bio.sourceforge.net/bowtie2/index.shtml |
| Picard MarkDuplicates | Broad Institute | https://github.com/metabrainz/picard |
| deepTools 3.3.0 | Ramírez et al.[55] | https://github.com/deeptools/deepTools |
| Trim Galore v0.5.0 | Felix Krueger | https://github.com/FelixKrueger/TrimGalore |
| Hisat2 v2.1.0 | Sirén, Välimäki and Mäkinen[56] | https://daehwankimlab.github.io/hisat2/ |
| featureCounts v1.6.4 | Liao et al.[57] | https://github.com/ShiLab-Bioinformatics/subread |
| Database for Annotation, Visualization and Integrated 6.7 Discovery (DAVID) | Sherman et al.[58] | https://david.ncifcrf.gov |
| clusterProfiler | Xu et al.[59] | https://github.com/YuLab-SMU/clusterProfiler |

## EXPERIMENTAL MODEL AND STUDY PARTICIPANT DETAILS

### Cells and cell culture

HEK293T (TaKaRa), A549 (NCACC) cell lines were cultured in DMEM (Gibco, 11965-118) media supplemented with 10% FBS (ExCell, FSP500). H1944 (NCACC) cell line was cultured in RPMI1640 (Gibco, 11875-119) supplemented with 10% FBS and 1 mM sodium pyruvate (Gibco, 11360070). All media were supplemented with penicillin and streptomycin (Gibco, 15140-122). Cells were cultured at 37°C with 5% $CO_2$, and were periodically tested and shown to be mycoplasma negative.

### Mice and animal procedures

All animal experiments were performed under strict compliance with the Institutional Animal Care and Use Committee (IACUC) of CAS Center for Excellence in Molecular Cell Science, Shanghai Institute of Biochemistry and Cell Biology (SIBCB), Chinese Academy of Sciences. All animal studies were performed according to protocols approved by the IACUC (Protocols: SIBCB-NAF-15-003-s202-013) and in accordance with the guidelines and ethical regulations of the IACUC.

*Kras*$^{LSL\text{-}G12D/+}$ mice (the Jackson Laboratory [JAX] stock No. 008179)[60] and *Rosa26*$^{LSL\text{-}tdTomato/+}$ mice (JAX stock No. 007909)[61] have been described previously. The schematic illustration of targeted disruption of *Ape1* in mice is shown in Figure S3C. *Ape1* conditional knockout mice were crossed with *Kras*$^{LSL\text{-}G12D/+}$ or *Kras*$^{LSL\text{-}G12D/+}$; *Rosa26*$^{LSL\text{-}tdTomato/+}$ mice to generate the mouse cohorts with desired genotypes used in this study. Mice were housed in the specific pathogen-free (SPF) animal facilities in a climate-controlled clean room with humidity range of 40–70% and temperature range of 20–26°C, with a 12-h light/dark cycle and fed with regular chow and water by the facility staff. All mice were maintained on C57BL/6 genetic background and adult mice were used in all studies. Both male and female mice were used in this study, and no significant influence of sex on the results was observed.

## METHOD DETAILS

### Generation and validation of CRISPR-KO/KI cell lines

We mainly followed the published protocol for CRISPR knockout using one or two distinct sgRNAs via transient transfection of pX330-mCherry vectors.[62] Following FACS sorting, mCherry positive single cells were plated into 96-well plate until knockout single clones emerged. The deletion of the sgRNA targeted region was validated by Sanger sequencing and all edited cell lines were further

validated for knockout efficiency by Western blotting. For knockin experiments, pX330-mCherry plasmid and repair dsDNA template amplified from the donor plasmid were transfected together. Gene name, sgRNA number and sequence are listed in Table S1.

### Cell viability assay

The cell viability at each individual time point was assessed with Cell Counting Kit 8 (Dojindo, CK04) according to the manufacturer's instruction. The absorbance at 450 nm was measured using the microplate reader (BioTek SynergyNEO). Three parallel wells were used per treatment and per time point.

### Cell-cycle analysis

Cells were collected and labeled using the BD Pharmingen™ FITC BrdU Flow Kit (BD, #559619). Both WT and APE1 knockout A549 cells were analyzed. For each sample, $10^4$ cells were measured by flow cytometry using FACS Jazz (BD, Heidelberg, Germany). All experiments were repeated at least twice.

### RNA-seq library preparation

For A549 cell line, RNA was extracted from $1 \times 10^6$ cells using TRIzol reagent (Invitrogen). 1 μg total RNA was used for the following library preparation. RNA-seq libraries were prepared with VAHTS mRNA-seq V3 Library Prep Kit for Illumina (Vazyme, NR611) according to the manufacturer's instructions. Libraries were sequenced as 151-base pair paired-end reads using an Illumina Novaseq 6000 by Genergy Biotechnology.

For premalignant cells, lung tissues with hyperplasia were dissociated at 12 wk after adenoviral infection, and $tdTomato^+/EPCAM^+/DAPI^-/CD45^-/CD31^-$ cells were prepared and sorted as described below (see FACS analysis).[34] Approximately 500 premalignant cells were lysed, and the reverse-transcribed RNA was preamplified to obtain enough cDNA by a modified SMART-Seq2 protocol.[63] cDNA was quantified by Qubit 4 (Invitrogen), and then 1 ng cDNA was used for DNA library construction with TruePrep DNA Library Prep Kit V2 for Illumina (Vazyme, TD503).

### RNA-seq data analysis

We mainly followed the published protocols for RNA-seq data analysis.[34] RNA-seq data were processed by trimming adapters and low-quality bases using Trim Galore (v0.5.0). Clean reads were mapped to the mouse mm10 or human hg38 genome using Hisat2 (v2.1.0).[56] Only uniquely mapped reads were retained. Gene count matrixes were calculated by featureCounts (v1.6.4)[57] and differential expression analysis was performed using DESeq2 ($P < 0.05$, fold change $\geq 2$). Gene Ontology (GO) and Kyoto Encyclopedia of Genes and Genomes (KEGG) pathway enrichment were conducted using Database for Annotation, Visualization and Integrated Discovery (DAVID) 6.7,[58] and gene set enrichment analysis (GSEA) was conducted using clusterProfiler package.[59]

### Quantitative real-time PCR analysis

For quantitative real-time PCR (qRT-PCR), total RNA was isolated from cells using the TRIzol (Thermo Fisher Scientific) method. $1–5 \times 10^6$ cells were used for total RNA extraction and 1 μg RNA from each sample was treated with DNase I and reverse-transcribed into cDNA by PrimeScript RT reagent Kit (Takara, RR047A). Quantitative real-time PCR was performed using Bio-Rad CFX96 with SYBR Premix Ex Taq (Takara, RR820). Fold change was calculated based on $2^{-\Delta\Delta Ct}$ method after normalization to the transcript level of the housekeeping gene *ACTB* or *GAPDH*. Primers for RT-qPCR are listed in Table S2.

### LC-MS sample preparation

The culture medium from the cultured cells ($\sim 10^7$ cells per sample) was removed using pipette. Then the cells were washed with PBS under room temperature and the PBS was removed. 1 ml of cold methanol/acetonitrile/water (2:2:1, v/v/v) was added to remove the protein and extract the metabolites. The mixture was collected into a new centrifuge tube, and centrifuged at 14000 g for 5 min at 4°C to collect the supernatant. The supernatant was dried in a vacuum centrifuge. For LC-MS analysis, the samples were re-dissolved in 100 μl acetonitrile/water (1:1, v/v) solvent.

### LC-MS analysis

To identify and quantify the concentration of L-arginine, L-citrulline and L-ornithine in cells, the analyses were carried out by Multi-reaction monitoring (MRM) mode of UPLC-QQQ-MS/MS (Agilent 1290/6495 tandem mass spectrum, Agilent USA). To identify these metabolites, authentic metabolite standards were used. An Acquity UPLC, BEH Amide 1.7μm, 2.1*100mm (Waters) was used for LC separation, using gradient elution with 0.1% formic acid acetonitrile as solvent A and 0.1% formic acid water as solvent B. The gradient program is as follows: 0–1 min 95% A, 1–15 min 95% A to 30% A, 15–16 min 30% A to 95% A, 16–25 min 95% A. The flow rate was set at 0.3 ml min-1, and the injection volume was 2 μl. A Jet Stream electrospray ESI ion source in positive ion mode was used to detect these three kinds of amino acids. Nitrogen generator (PEAK Shanghai) was used for solvent removal and atomization, and high purity nitrogen as colliding gas. Sheath Gas Temp is 280°C, Sheath Gas Flow flows at 11 L / min, Gas Temp is 200°C and Gas Flow is 11 L /min. Capillary voltage is 3500 V, Nebulizing Gas is 25 psi, Nozzle Voltage is 500 V. Selected

ions for ornithine, citrulline and arginine are described as following. Precursor ion (m/z): 133.1, 176.1 and 175.1; Products ion (m/z): 70.1, 159 and 70.2; Fragmentors: 80, 80 and 100; CE: 20, 5 and 25.

For untargeted metabolomics of polar metabolites, extracts were analyzed using a quadrupole time-of-flight mass spectrometer (Sciex TripleTOF 6600) coupled to hydrophilic interaction chromatography via electrospray ionization in Shanghai Applied Protein Technology Co. Ltd. (Shanghai, China). Metabolites with a variable importance in projection value >1 were evaluated using Student's t-test. $p < 0.05$ was considered to indicate statistically significant results.

### Fluorometric measurement of cellular ammonium content

$1 \times 10^6$ cells were harvested and then washed twice using UPLC water to remove any residual traces of ammonium. After the second wash, the supernatant was discarded and pellets were snap frozen in liquid nitrogen and stored at −80°C until further analysis. The extraction of ammonium was performed by resuspending the pellets in 200 μl of UPLC water, followed by exposure to three freeze-thaw cycles. The lysate was centrifuged for 240 min at 3,000,000 g at 4°C and the supernatant was aliquoted for ammonium assay. The ammonium content was measured using ammonium assay kit (Sigma-Aldrich, MAK310) as per the vendor's instructions.

### Western blotting analysis

Cells were collected and lysed by ProteinExt Mammalian Total Protein Extraction Kit (Transgen, DE101). The whole cell extracts were heated at 100°C before loading to SDS–PAGE gels. Western blotting was performed as described previously.[64] The blots were detected with SuperPico ECL Chemiluminescence Kit (Vazyme, #E422) and images were obtained using MiniChemi® 580 Chemiluminescence Imaging System (SAGECREATION). The primary antibodies used in this study included anti-APE1 (Abcam, ab194, 1:2,000), anti-CPS1 (ABclonal, A19978, 1:1,000), anti-FLAG (Sigma, F1804, 1:5,000), anti-HA (Cell Signalling Technology, 3724, 1:1,000), anti-KRAS (Sigma, WH0003845M1, 1:500), anti-β-actin (ABclonal, AC026, 1:10000). Secondary antibodies used included HRP conjugated goat anti-mouse IgG (Jackson, 115-035-003, 1:10,000) and goat anti-rabbit IgG (Jackson, 111-035-003, 1:10,000).

### Generation of the Ape1 knockout and N211A mutant mice with CRISPR/Cas9-mediated gene editing technology

We mainly followed the published protocols for CRISPR/Cas9-mediated gene editing.[62,65–67] The *Ape1* gene was inactivated by targeting exons 2–3. For the generation of APE1 catalytically inactive mice, the Asn211 encoded by the fifth exon of the *Ape1* gene is mutated to Ala. The schematics of targeted disruption and N211A point mutation of Ape1 are shown in Figures S3C and S3E. The sgRNA target sites and oligonucleotides are available in Table S1. For microinjection of one-cell embryos, B6D2F1 female mice and ICR mice were used as embryo donors and foster mothers, respectively. The embryo-donor female mice were superovulated and mated with wild-type male mice. One-cell-stage embryos were collected from oviducts and injected into the cytoplasm with Cas9 mRNA (100 ng/μl), sgRNA (50 ng/μl) and oligo donors (50 ng/μl) in RNase-free water using an Eppendorf TransferMan NK2 micromanipulator. The injected embryos were cultured in KSOM at 37°C under 5% $CO_2$ until the 2-cell stage and transferred into oviducts of pseudopregnant ICR females at 0.5 dpc. The genotyping of mice was performed as described previously,[67] PCR primers are listed in Table S3.

### H&E staining, immunohistochemistry and immunofluorescence analysis

H&E staining and immunohistochemistry of paraffin-embedded tumor-bearing lung sections were performed following the published protocol.[34] Primary antibody against ARG2 (Cell Signaling, 55003, 1:2000) was used in this study. Histological slides were scanned with a Zeiss Axio Zoom V16 stereoscope, and photomicrographs were captured on an Olympus BX51 microscope.

To stain cells in culture, cells were seeded on glass slides and cultured for 24 h. Then we performed immunostaining as described previously.[34] Primary antibody against Phospho-Histone H2A.X (Ser139) (20E3) (Cell Signaling, 9718, 1:400) and secondary antibody Cy3 goat anti-rabbit IgG (Jackson ImmunoResearch, 111-165-144, 1:1,000) were used. Nuclei were counterstained with DAPI (BBI, E607303). Immunostained images were obtained using a confocal fluorescence microscope (Zeiss LSM880) with objective magnification of ×63.

### FACS analysis

Mice with LUAD tumors were euthanized at 12 wk after adenoviral infection. LUAD cells were prepared following the published protocol at $1 \times 10^6$/100 μl.[34] To isolate primary LUAD cells from *Kras*$^{LSL\text{-}G12D/+}$, *Kras*$^{LSL\text{-}G12D/+}$; *Ape1*$^{flox/+}$, *Kras*$^{LSL\text{-}G12D/+}$; *Ape1*$^{flox/flox}$ and *Kras*$^{LSL\text{-}G12D/+}$; *Ape1*$^{flox/N211A}$ tumors, the cells were stained with the antibodies anti-CD45 APC (BioLegend, 103112, 1:100), anti-CD31 APC (BioLegend, 102510, 1:100), and anti-CD326 (EPCAM) APC/Cy7 (BioLegend, 118218, 1:100). DAPI as a viability dye (BD Bioscience, 564907) was added to each sample to identify dead cells before FACS sorting. Single staining controls and fluorophore minus one control were included for each experiment. *DAPI*$^-$/*CD45*$^-$/*CD31*$^-$/*tdTomato*$^+$ live cells were sorted using a BD FACS Aria Special Order Research Product (SORP), and analysis was done with FlowJo (v10.0.7).[68–70]

### ChIP–qPCR

We performed ChIP-qPCR as described previously.[32] Briefly, 2 × $10^7$ A549 cells with HA-tagged Ape1 were collected, crosslinked with 1% formaldehyde for 10 min at room temperature and quenched with 0.125 M glycine. The final DNA length was approximately 300 bp sonicated using a COVARIS S220. The sonicated chromatin supernatant was divided into two equal parts: one for HA and FLAG antibody, the other for normal IgG to serve as a negative control. 1/10 of the supernatant was incubated with the anti-HA (Cell Signalling Technology, 3724, 1:50), anti-FLAG (Sigma, F1804, 1:50) antibody at 4°C overnight and immunoprecipitation was performed with Protein G magnetic beads. Immunoprecipitated chromatin (ChIP DNA) was eluted in TE buffer. For each sample, input, ChIP DNA and IgG were used for qPCR to determine the enrichment of indicated genes. Primer sequences used for ChIP qPCR are provided in Table S2.

### Circular dichroism spectroscopy

Circular dichroism (CD) spectra were obtained on a Chirascan V100 CD spectrometer, equipped with 10 mm 3,500 μl one-piece stoppered cuvette. The instrument was controlled by Chirascan Control and Chirascan Viewer software. The Active Nitrogen Management System (ANMS) for monitoring and control of nitrogen purging runs independently of the Chirascan software. Single-stranded and double-stranded oligonucleotide solutions were annealed in 30 mM Tris-HCl (pH 7.5) with 15 mM KCl, 150 mM KCl or 150 mM LiCl by heating at 95°C for 5 min followed by slow cooling to room temperature. Scans were performed over the range of 220 to 320 nm at 20°C in duplicate. The spectra were recorded in a 10 mm quartz cuvette at 20°C. The methods of scan and statistics are performed as described previously.[32]

### Thermal difference spectra

TDS was performed essentially as described.[39] Thermal denaturation was performed with a Cary 100 Bio UV-Visible Spectrophotometer and 1 cm path-length quartz cuvette. The UV spectra were measured over a 220–335 nm spectral range at a 1 nm data interval. Spectra were recorded at 20°C, the sample was then heated to 90°C. Data was normalized and plotted vs. wavelength using GraphPad Prism 10.

### Cleavage under targets and tagmentation (CUT&Tag)

CUT&Tag was performed essentially as described,[71] with minor modifications according to the Hyperactive Universal CUT&Tag Assay Kit protocol (Vazyme, TD904). *APE1*$^{+/+}$, *APE1*$^{-/-}$, *ARG2*$^{MUT}$ and *CPS1*$^{MUT}$ A549/H1944 cells (1 × $10^6$) were used for the CUT&Tag experiment, and cell counting was performed using a Luna II (Logos Biosystems, Korea). The G4 antibody BG4 was kindly provided by Prof. Kaiwei Liang. The H3K4me3 antibody (Abcam, ab8580, 1:50) was used in this assay.

The CUT&Tag reads were mapped to the human genome (UCSC hg38) with Bowtie2 2.3.1.[54] The duplicated reads were removed with Picard MarkDuplicates, and the deduplicated BAM files were normalized to the total aligned reads (reads per genome coverage, RPGC) with the bamCoverage command from deepTools 3.3.0.[55]

### ATAC-seq

ATAC-seq was performed as described,[72] with minor modifications according to the TruePrepTM DNA Library Prep Kit V2 protocol (Vazyme, Nanjing, China). ATAC-seq libraries were sequenced on Illumina HiSeq6000. The ATAC-seq reads were mapped to the human genome (UCSC hg38) with Bowtie2 2.3.1.[54] The duplicated reads were removed with Picard MarkDuplicates, and the deduplicated BAM files were normalized to the total aligned reads (reads per genome coverage, RPGC) with the bamCoverage command from deepTools 3.3.0.[55]

### Bio-layer interferometry assay

Bio-layer interferometry assays were performed using a ForteBio Octed RED96 with protein, oligonucleotides, and streptavidin (SA) biosensors (Octed, 18-5019). The purified human APE1 protein was kindly provided by Cytosinlab Therapeutics. Biotin-labeled CPS1 G4 oligonucleotide (5′-[Biotin] TTG TCC GGG TGG GTT AAG GGC CCT G-3′), CPS1 MUT oligonucleotide (5′-[Biotin] TTG TCC GAG TGA GTT AAG AGC CCT G-3′), ARG2 G4 oligonucleotide (5′-[Biotin] GGG GGA CCG GGA GGC GAG GAG AGG ATG GG-3′), ARG2 MUT oligonucleotide (5′-[Biotin] GGA GTA CCG TGA GAC GAG TAG AGT ATG AG-3′) and MYC G4 oligonucleotide (5′-[Biotin] TGA GGG TGG GTA GGG TGG GTA-3′) were synthesized by Sangon Biotech. Synthetic single-stranded DNA oligos were induced to form G4 structures by incubating 10 μM oligos in annealing buffer (final volume: 100 μL) at 95°C for 5 minutes, followed by gradual cooling to 37°C. For double-stranded DNA templates, 10 μM of each complementary strand was annealed under the same conditions. Kinetic titration series were performed in the interaction buffer (25 mM HEPES, pH 7.5, 1.25 mM MgCl2, 150 mM KCl, 0.1% v/v Igepal CA-630, 1 mM DTT). Purified protein APE1 were serially diluted with the interaction buffer from 500 to 31.25 nM. The SA biosensors were hydrated in the interaction buffer for 10 min at 25°C. Following the initial 60-s baseline, the SA biosensors were loaded with the biotin-labeled G4 for 360 s. Redundant probes were removed by a 120-s baseline adjustment. To measure the interaction between protein and G4s, the duration time of association and dissociation was set to 300 s. Sensorgrams and sensor signals were analyzed by the Octet Data Analysis 9.0 software.

## QUANTIFICATION AND STATISTICAL ANALYSIS

Statistical analyses were performed using GraphPad Prism v.10.1.1. All data are represented as mean ± SEM of individual data points from three or four independent biological replicates. Two-tailed unpaired Student's *t* test, $\chi^2$ test, log-rank (Mantel–Cox) test, and one-sided Fisher's exact test were used to determine statistical significance. In all types of statistical analysis, values of $P \leq 0.05$ were considered significant. ns, not significant. *N* values and statistical method used in each experiment are indicated in the figure legends or in the figure themselves.